Flinders
UNIVERSITY

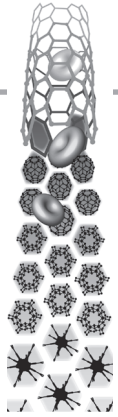

Controlled drug delivery from composites of nanostructured porous silicon and poly(L-lactide)

Aims: Porous silicon (pSi) and poly(L-lactide) (PLLA) both display good biocompatibility and tunable degradation behavior, suggesting that composites of both materials are suitable candidates as biomaterials for localized drug delivery into the human body. The combination of a pliable and soft polymeric material with a hard inorganic porous material of high drug loading capacity may engender improved control over degradation and drug release profiles and be beneficial for the preparation of advanced drug delivery devices and biodegradable implants or scaffolds. **Materials & methods:** In this work, three different pSi and PLLA composite formats were prepared. The first format involved grafting PLLA from pSi films via surface-initiated ring-opening polymerization (pSi–PLLA [grafted]). The second format involved spin coating a PLLA solution onto oxidized pSi films (pSi–PLLA [spin-coated]) and the third format consisted of a melt-cast PLLA monolith containing dispersed pSi microparticles (pSi–PLLA [monoliths]). The surface characterization of these composites was performed via infrared spectroscopy, scanning electron microscopy, atomic force microscopy and water contact angle measurements. The composite materials were loaded with a model cytotoxic drug, camptothecin (CPT). Drug release from the composites was monitored via fluorimetry and the release profiles of CPT showed distinct characteristics for each of the composites studied. **Results:** In some cases, controlled CPT release was observed for more than 5 days. The PLLA spin coat on pSi and the PLLA monolith containing pSi microparticles both released a CPT payload in accordance with the Higuchi and Ritger–Peppas release models. Composite materials were also brought into contact with human lens epithelial cells to determine the extent of cytotoxicity. **Conclusion:** We observed that all the CPT containing materials were highly efficient at releasing bioactive CPT, based on the cytotoxicity data.

Original submitted 16 December 2010; Revised submitted 29 September 2011; Published online 6 March 2012

KEYWORDS: composite material ■ glaucoma ■ localized drug delivery ■ poly(L-lactide) ■ porous silicon ■ uveitis

Steven JP McInnes[1], Yazad Irani[2], Keryn A Williams[2] & Nicolas H Voelcker*[1]

[1]Flinders University, School of Chemical & Physical Sciences, Adelaide, Australia
[2]Department of Ophthalmology, Flinders University, Adelaide, Australia
**Author for correspondence: Tel.: +61 8 8201 5338 nico.voelcker@flinders.edu.au*

The therapeutic effects of existing, common drugs can be enhanced via the use of controlled drug delivery systems. Hence, the development of new delivery systems is often considered as a commercially viable alternative to the expense of drug discovery and development [1–3]. Controlled drug delivery systems have now been developed to the point where they can facilitate site-specific delivery at precisely controlled rates [4–9]. Control over the delivery rate minimizes the toxicity and side effects of the drug being delivered [1,10–15]. In order for a drug delivery system to provide a therapeutic payload with the maximum therapeutic benefit, the release profile of new drug delivery systems typically need to be carefully adapted to the particular application.

Our current research goal is to develop new vehicles for localized transfer of drugs to the anterior segment of human eyes affected by the sequelae of ocular inflammation. For example, uveitis, defined as inflammation of the uveal tract, has an estimated prevalence of 17 per 100,000 population and is responsible for 10% of all cases of serious visual loss in developed countries [16]. These conditions are typically treated with topical and oral glucocorticosteroids. In spite of these drugs being associated with significant side effects and often insufficiently control acute or recurrent inflammation, they remain the mainstay of current treatment. Additional systemic immunosuppression with agents such as methotrexate or cyclophosphamide may then be required [17]. However, these drugs must be administered daily and their side effects, although manageable, are not trivial [18]. Another targeted disease, primary open-angle glaucoma, has a prevalence of 1–4% in different populations and is the second most common cause of blindness in the developed world [19]. Treatment consists of reducing intraocular pressure with drugs or surgery designed to increase outflow of aqueous humor from

Future Medicine part of fsg

the eye [20,21]. To reduce fibrosis after surgery, cytotoxins may be applied to the eye repeatedly, but this procedure can cause damage to the extraocular tissues.

A biomaterial that can support localized and sustained drug delivery to the cornea and anterior segment of the eye may prove a safe and effective method of delivery and improve existing therapeutic options in patients affected by acute anterior uveitis or glaucoma. Similar considerations apply to conditions, such as corneal neovascularization, that follow the inflammation caused by trauma or infectious keratitis, or that may accompany ocular surface disease [22]. Local delivery of an antiangiogenic agent loaded into a biodegradable material might well be a viable therapeutic option.

Silicon (Si)-based materials, including silicones, silica, porous Si (pSi) and micromachined crystalline Si are commonly used in drug delivery because they are relatively bioinert [23,24]. Fabricating pSi films from single crystalline Si is achieved by an electrochemical etch in electrolyte mixtures of aqueous hydrofluoric acid (HF) and ethanol. Changes to wafer resistivity and process parameters such as electrolyte concentrations and current densities allow for the generation of a wide range of pore sizes and structures [25]. pSi has key advantages because, unlike flat Si, it degrades completely in aqueous solutions into nontoxic silicic acid [25], the major form of Si in the environment and human body [24], and is proving to be remarkably inert and noninflammatory within the body [26]. The material has a very high surface area (400–800 m^2/g) [25], a property essential for high drug loading regimes. Since the material is insoluble in organic solvents, loading of a wide range of small-molecule drugs with different solubilities is possible. Also, in contrast to most polymeric materials, the surface chemistry of pSi can be modified by simple one-step chemical treatments without affecting its material properties. Surface modification allows tuning of the loading and release characteristics of a wide range of bioactives [27–30]. Depending on the chemical doping of the Si material base, etching conditions and surface modification [31–33], the degradation kinetics can be controlled from hours to months. Finally, recent reports have shown that the photonic properties of pSi allow self-reporting of drug loading and release [7,34]. An additional benefit associated with the use of pSi is that it can be processed into films supported on Si, free-standing membranes and micro- or nano-particles [32,34–38].

Polymeric drug delivery devices and systems have proved invaluable in enhancing the therapeutic efficacy of drugs, while reducing toxicity and enhancing patient compliance [39]. One popular biodegradable polymer class for drug delivery is the polyesters, which include polylactides, poly(ε-caprolactone), poly(3-hydroxybutyrate and poly(glycolic acid) [40]. These polymers and various copolymer compositions have shown considerable potential as effective drug carriers [41,42] and have been extensively studied for the controlled release of drugs due to their tunable degradation rates (from months to years), wide range of mechanical properties and biodegradability [40,43–49]. Poly(L-lactide) (PLLA) is particularly advantageous since its degradation product, lactic acid, is well tolerated by the body [50–53]. The degradation properties of polyesters have been widely studied [54,55] and are known to be affected by polymer properties (i.e., molecular weight, chemistry, wettability and crystallinity) and also the properties of the release medium (i.e., pH, ionic strength and solvent) [56].

We have previously demonstrated that composite membranes of pSi and poly(ε-caprolactone) can be implanted successfully into the subconjunctival space of the rat eye, without obscuring the visual axis [37,57]. These materials did not erode the under- or overlying tissue, did not cause any significant accumulation of acute inflammatory cells around the insert, did not become vascularized and remained visible with the operating microscope for periods over 8 weeks. Eventually, the membranes dissolved without a trace, leaving behind a small, encapsulated space. Human lens epithelial cells and primary human corneal explants adhered to the membranes, where they remained viable and underwent division.

Here, we investigated the properties of composite materials of pSi and PLLA as advanced materials for controlled drug release, combining the useful drug release properties of pSi with the good processability of PLLA. In particular, we prepared three different formats of composites (Figure 1) using surface-initiated polymerization to graft PLLA to pSi (pSi–PLLA; grafted), spin-coating of bulk polymerized PLLA onto pSi films (pSi–PLLA; spin-coated) and pSi–PLLA monoliths prepared by mixing of pSi microparticles into a molten PLLA matrix. Based on our previous work, we speculate that the resulting films and monoliths can be implanted into the subconjunctival space. Others have demonstrated that pSi particles can be injected into the vitreous for drug delivery to the posterior chamber of the

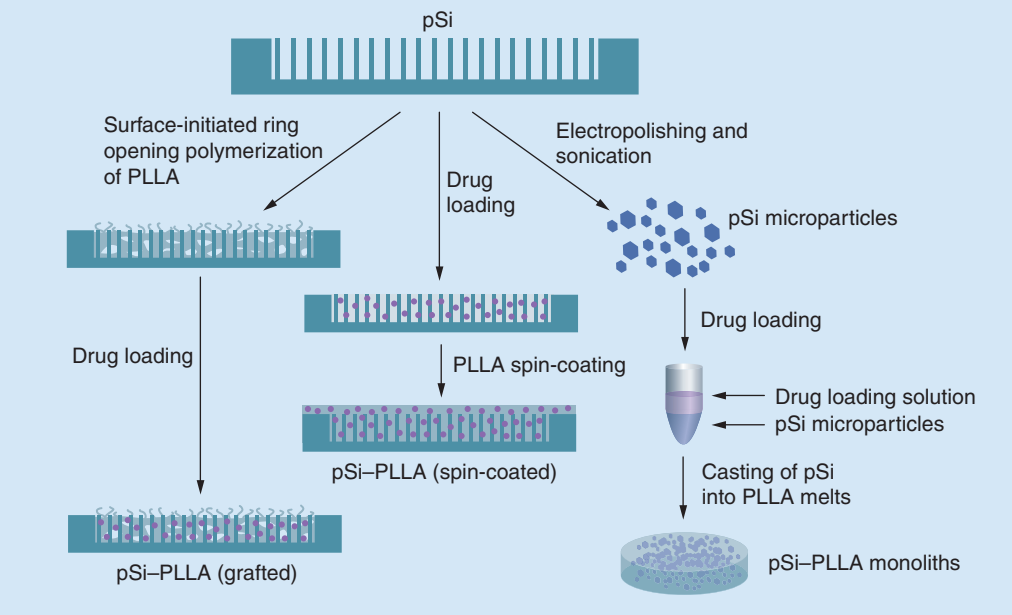

Figure 1. Drug loading of porous silicon films and microparticles, and generation of porous silicon and poly(L-lactide) composite materials.
PLLA: Poly(L-lactide); pSi: Porous silicon.

eye [57]. We examined the composite materials' ability to release a model drug, the cytotoxic topoisomerase inhibitor camptothecin (CPT), and investigated cytotoxicity *in vitro* and determined that all three composite formats show release behavior that is compatible with localized drug delivery to the ocular surface.

Materials & methods

Chemicals

Dichloromethane (CH_2Cl_2, Merck, NJ, USA) and toluene (Aldrich, MO, USA) were distilled over calcium hydride and stored over molecular sieves away from light. Tetrahydrofuran (THF) was distilled over sodium and benzophenone and stored over molecular sieves away from light. L-lactide ([3S]-*cis*-3,6-dimethyl-1,4-dioxane-2,5-dione; 98%, Aldrich) was recrystallized before use. Polyethylene glycol (PEG) 6000 (average molecular weight 6000–7000 g/mol, 130–170 repeats with hydroxyl terminal functionality), HF 48% (BDH/Merck, Darmstadt, Germany) and tin(II) 2-ethylhexanoate ($Sn(Oct)_2$i; 95%, Aldrich) were used as received. (S)-(+)-CPT (CPT, Aldrich, 95%) was stored at 2–4°C and protected from light at all times. Methanol (Merck, analytical grade, 99.5%), acetone (Ajax, NSW, Australia, analytical grade, 99.5%) and ethanol (Ajax, absolute, 100%) were used for etching and washing without further purification. *N*,*N*-dimethylformamide (DMF) was purified via standard laboratory protocols including drying over magnesium sulfate followed by distillation at reduced pressure [58]. MilliQ® water 18.2 MΩ was obtained from a Labconco (MO, USA), Water Pro PS water purifier. Phosphate-buffered saline (PBS), pH 7.4, was prepared in MilliQ water from sodium chloride (analytical grade, Chemsupply, Port Adelaide, Australia, 99.0%; 136.9 mM), potassium chloride (analytical grade, Biolab Scientific, Auckland, New Zealand, 99.5%; 2.68 mM), disodium phosphate di-hydrate (AR, Chemsupply, 99.0%; 3.71 mM) and potassium dihydrogen orthophosphate (analytical grade, Ajax, 99.0%; 1.76 mM). The pH was adjusted by buffering with 1 M solutions of sodium hydroxide (Ajax, analytical grade) or hydrochloric acid (Aldrich, reagent grade) in MilliQ water.

Production & loading of pSi–PLLA (grafted) composite materials

Production of pSi films

For infrared (IR) studies, p^+ type Si wafers (Silicon Quest International, NV, USA; boron doped, 381 ± 25 µm, resistivity of 3–6 Ωcm, <1–0–0>) were etched in 1:1 HF:ethanol electrolyte at a current density of 36.67 mA/cm^2 using a etching cell with an exposed area of 1.8 cm^2. The pSi films were then washed with copious amounts of methanol, ethanol, acetone and finally CH_2Cl_2 and dried in a stream of N_2. Ozone oxidation was performed using a Fischer® OZON, Ozon-Generator 500 (Fischer America, São Paolo, Brazil). All oxidations were performed at an ozone rate of 3.25 g/h.

Surface silanizations

N-(hydroxyethyl)-3-aminopropyl trimethoxysilane (HEAPS) and *N*-(triethoxysilylpropyl)-*O*-polyethylene oxide urethane (PEGS) were purchased from Gelest Inc. (VA, USA), and used as received. Surface treatments with HEAPS and PEGS silanes were carried out on oxidized pSi (pSi-Ox) surfaces at room temperature for 10 min by submersion in an anhydrous solution of silane in toluene (50 mM). Afterwards, the surfaces were rinsed with toluene, acetone and CH_2Cl_2 and dried under a stream of N_2.

Ring-opening graft polymerization of PLLA

Oxidized and silanized pSi films were soaked in 10 ml of toluene containing 5 µmol $Sn(Oct)_2$ catalyst for 1 h at 50°C before addition of 10 mmol (1.44 g) of recrystallized L-lactide. The polymerization reaction proceeded for 72 h at 110°C. Upon completion of the polymerization, the pSi films were removed and washed with toluene, acetone and CH_2Cl_2 before being treated by Soxhlet extraction in anhydrous toluene for 30 min. All pretreatments, polymerizations and washing procedures were carried out under an N_2 atmosphere.

CPT loading of PLLA-grafted pSi films

PLLA-grafted pSi films (1.8 cm^2) were placed into 10 ml of a solution of 2.5 mg/ml CPT (Aldrich, 95%) in dry distilled DMF for 2 h before being removed and dried under vacuum (10 mm/Hg) in a desiccator.

Production & loading of pSi–PLLA (spin-coated) composite materials

Bulk polymerization of PLLA

A total of 5 g of recrystallized L-lactide was heated above its melting point (~140°C) and 1 wt% of $Sn(Oct)_2$ catalyst was added to the melt and stirred for 4 h to allow for polymerization. Upon completion of the polymerization, the polymer block was put through a Soxhlet extraction for 2 h with toluene to remove any remaining catalyst. The cooled solid block of PLLA was manually pulverized into a fine white powder.

Spin coating of PLLA

pSi-Ox films (1.8 cm^2) were loaded as described under the section 'CPT loading of PLLA grafted pSi films', but a higher concentration of CPT (10 mg/ml) was used in order to compensate for the removal of CPT by THF during the spin coating process. Spin coating was performed using a WS-400B-6NPP/LITE model spin coater (Laurell Technologies Corporation, PA, USA) at 5000 rpm with a solution of 0.22 mg/ml PLLA in THF at 80°C on CPT-loaded pSi films. Once dried, the surfaces were removed from the spin coater and placed on a hotplate at 200°C for 10 s to further assist the infiltration of the molten PLLA into the pores.

Production & loading of PLLA monolith composite materials

Fabrication of pSi microparticles

Microparticles were fabricated from p^{++} Si wafers (boron doped, resistivity <0.001 Ω cm, <1–0–0>) supplied by Virginia Semiconductors (VA, USA) using a custom-built, 18-cm^2 teflon etching cell. The wafer was anodized in 3:1 HF:ethanol solution with a density of 111 mA/cm^2 for 4 min and then electropolished for 30 s at 500 mA/cm^2. CH_2Cl_2 was then added, and the free-standing porous layer was manually fractured into microparticles for collection. The pSi microparticle suspension was sonicated for 20 min (to reduce the particle size) before being filtered and washed with ethanol and CH_2Cl_2. Ozone oxidation was performed as described above after an overnight incubation in an 80°C oven.

Production & loading of pSi–PLLA monoliths

Monoliths were produced by placing bulk polymerized PLLA into a casting plate, consisting of circular holes (3 mm in depth and 3 mm in diameter) and heating the material to just above the melting point of the PLLA (~170°C, for 10 s). The material was then slowly cooled to room temperature (over 5–10 min) before the monoliths were removed from the mould. To facilitate easy removal of the monoliths, 5% w/w of PEG 6000 was added as a plasticizer during the melt casting. Three different monolith formulations were produced:

- PLLA only: PLLA and PEG plasticizer (95:5 w/w);
- PLLA–CPT: 0.2 mg of CPT per 50 mg of PLLA:PEG (95:5 w/w);
- pSi–PLLA–CPT: the pSi microparticles preloaded with approximately 1 mg of CPT per 50 mg of pSi (prepared as described below) were subsequently mixed into 250 mg of PLLA:PEG (95:5) to give a final loading of 0.2 mg of CPT per 50 mg of PLLA:PEG (95:5 w/w).

As each monolith weighed approximately 76.5 ± 0.3 mg, the average loading of each monolith was approximately 0.31 mg or 878.4 ± 3.9 nmol of CPT.

The CPT-loaded pSi microparticles were prepared by adding 500 µl of 2.5 mg/ml CPT solution (in dry distilled DMF) to an Eppendorf tube containing approximately 50 mg pSi. After 2 h, the excess CPT solution was removed from the Eppendorf tubes and the microparticles were completely dried in a desiccator under vacuum conditions (0.5 mm/Hg). The final loading of microparticles was calculated gravimetrically as 2.87 µmol of CPT per 50 mg of pSi (or 1 mg CPT per 50 mg pSi). These particles were then loaded into PLLA monoliths (as described above for pSi–PLLA–CPT monoliths).

The pSi–PLLA nomenclature was chosen for the monolith composites (*cf.* the pSi–PLLA [grafted] and pSi–PLLA [spin-coated]) since PLLA is the major component of these materials, rather than pSi.

This fabrication incorporates high-temperature processing. However, we expect there to be little damage to the CPT as the maximum temperature of 170°C is only applied for a short time period (~10–20 s) and is well below the 260°C decomposition point of CPT [59,60].

Analysis techniques

Interferometric reflectance spectroscopy

Interferometric reflectance spectroscopy measurements were performed to determine the porosity of the pSi films. Briefly, reflectivity data were recorded for wavelengths between 400 and 1000 nm, with an acquisition time of 100 ms on a USB2000 spectrophotometer (Ocean Optics, FL, USA). To obtain the effective optical thickness of the pSi films, a fast Fourier transform was applied using the IGOR program (Wavemetrics, OR, USA). The effective optical thickness obtained with the dry films and the film filled with ethanol were modeled with a two-component Bruggeman effective medium model. This allowed for the porosity of the films to be calculated. The refractive indices for air, ethanol and pSi used in the model are 1.00, 1.36 and 2.05, respectively. Separate gravimetric measurements were performed on all samples to determine porosity and thickness.

Size exclusion chromatography

Size exclusion chromatography was performed on a system comprising a 2690-separation module (Waters, MA, USA) equipped with a Styragel® HR4E column (300 × 4.6 mm; Waters) providing an effective molecular weight range of 50–100,000 g/mol. A 410-refractive index detector (Waters) and a 996-photodiode array detector (Waters) were coupled in series. The eluent was THF with a flow rate of 0.3 ml/min. Number- and weight-average molecular weights were evaluated using Waters Millennium software and polystyrene standards. A polynomial was used to fit the log M versus time calibration curve, which was linear across the molecular weight range.

Thermal gravimetric analysis

Thermal gravimetric analysis (TGA) experiments were conducted under N_2 conditions at a flow rate of 50 ml/min on a SDT 2960 (TA Instruments, DE, USA). The temperature was ramped from room temperature to 550°C at 10°C/min. Each sample was accurately weighed by the TGA before measurements were performed, and all samples' weights ranged from 10 to 11 mg for consistency.

Water contact angle

Water contact angles (WCAs) were measured by placing a 1-µl drop of water on the sample surface and capturing a digital image using a Super Dynamic wv-BP550 Closed Circuit TV camera (Panasonic, NSW, Australia). The contact angle measurements were analyzed by Scion Image for Windows frame grabber software (beta version 4.0.2). Three replicate measurements were performed for each sample.

IR spectroscopy

All IR spectra were obtained using a Nicolet Avatar 370MCT (Thermo Electron Corporation, MA, USA) equipped with a standard transmission accessory. Spectra of the pSi films were recorded and analyzed using OMNIC™ Version 7.0 software (Thermo Electron Corporation), in the range of 650–4000 cm^{-1} at a resolution of 4 cm^{-1}. A background spectrum was taken on an unetched Si wafer.

Scanning electron microscopy

Scanning electron microscopy (SEM) was performed on either a XL30 field emission SEM (acceleration voltage of 10 kV; Philips, Holland) or a Phenom benchtop SEM (acceleration voltage of 2 kV; FEI, OR, USA). To help facilitate the dissipation of charge build-up, all samples (except the microparticles) were coated with a 5-nm thick layer of Pt before analysis, according to our standard laboratory protocol [37].

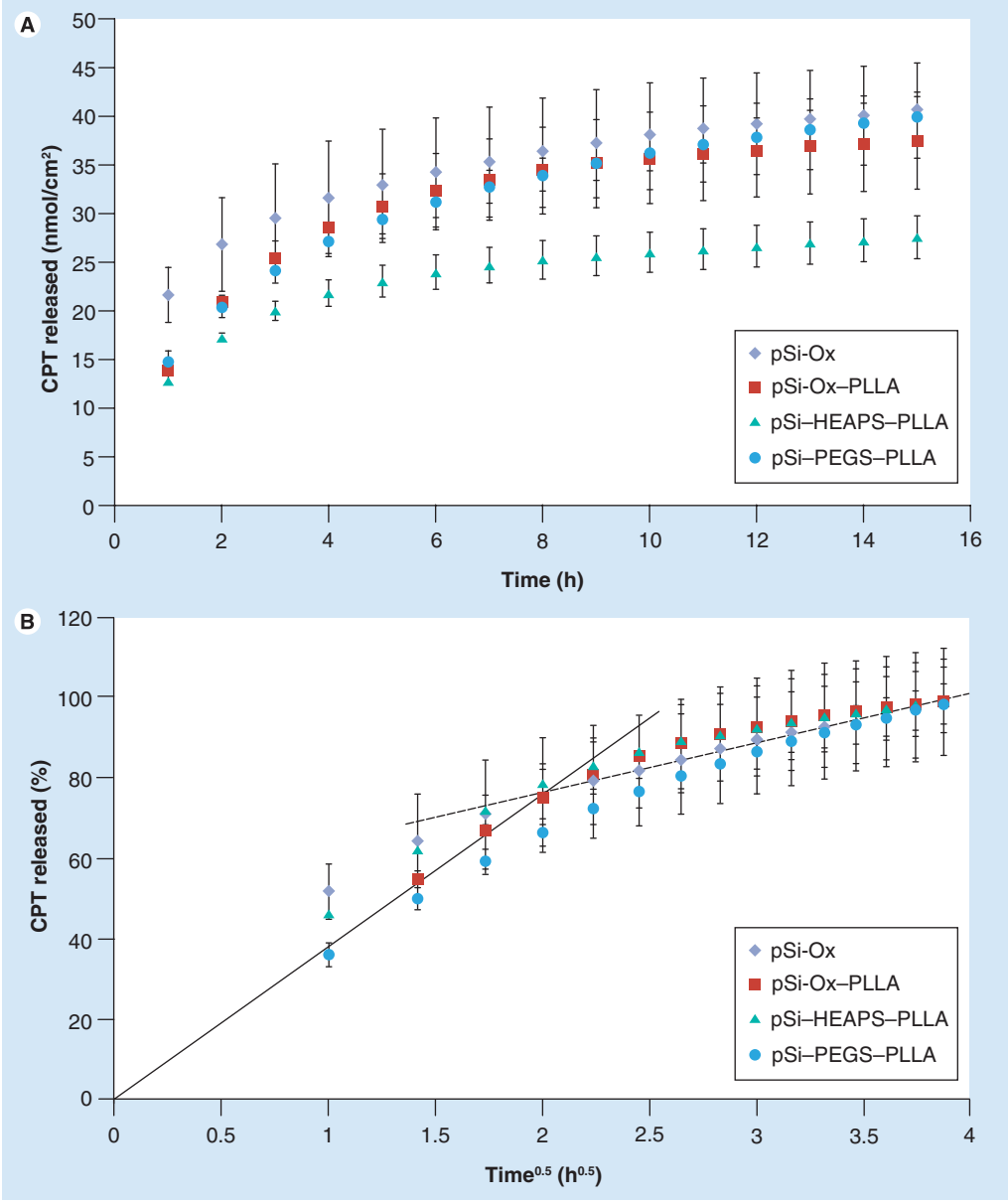

Figure 2. Drug release from porous silicon–poly(L-lactide; grafted) surfaces. (A) Release curves of CPT from grafted pSi–PLLA composite materials and **(B)** corresponding Higuchi plot of CPT release.
CPT: Camptothecin; HEAPS: *N*-(hydroxyethyl)-3-aminopropyl trimethoxysilane; Ox: Oxidized; PEGS: *N*-(triethoxysilylpropyl)-*O*-polyethylene oxide urethane; PLLA: Poly(L-lactide); pSi: Porous silicon.

Atomic force microscopy

Tapping mode atomic force microscopy (AFM) was performed on a Multimode Nanoscope with a Nanoscope IV controller (Veeco Corporation, CA, USA). Commercial Si cantilevers (FESP) acquired from Veeco Corporation with the following specifications were used for all experiments: beam shaped, 225 µm length, 28 µm width, 3 µm thickness, 2.8 N/m force constant, 75 kHz resonance frequency and a tip height and radius of 10–15 µm and <8 nm, respectively. All AFM was performed at ambient conditions and the images were processed and analyzed using the Nanoscope 5.31r1 software (Veeco Corporation).

CPT release assay by fluorimetry

The ability of the composite materials to release their CPT payload into 3 ml of static (unstirred) solution of PBS (pH 7.4) at 37°C was analyzed using a time-drive program and a standard quartz cuvette to collect fluorescence data. Fluorimetry was performed on a LS55 luminescence spectrometer (Perkin Elmer Instruments, MA, USA) with an excitation wavelength of

340 nm and emission wavelength of 434 nm, the slit width was 3 nm and the photomultiplier voltage was 775 V. The release cuvettes were sealed with Teflon® (DuPont Co., DE, USA) stoppers to prevent evaporation during the release period. Release rates were calculated from the slope of release curves obtained. The CPT-loaded pSi films were cut into smaller chips (chip areas varied between 0.1 and 0.2 cm^2) and the actual amount of CPT released was calculated via the use of a calibration curve and normalized relative to the chip area (not the pSi surface area) to determine the amount of CPT released per cm^2 of pSi chip. This procedure enabled easy comparison of the release data. A minimum of two release curves were averaged to give the curves shown in Figures 2–4. Despite the very low solubility of CPT in aqueous solutions (14.2 ± 2.9 µM) [61], sink conditions were maintained for all release experiments by ensuring that the maximum release concentrations were less then 1.4 µM. This was confirmed experimentally by assaying a 10× dilution of a solution saturated with CPT (in PBS at pH 7.4 and 37°C). This solution gave a fluorescence reading with values very similar to undiluted release runs

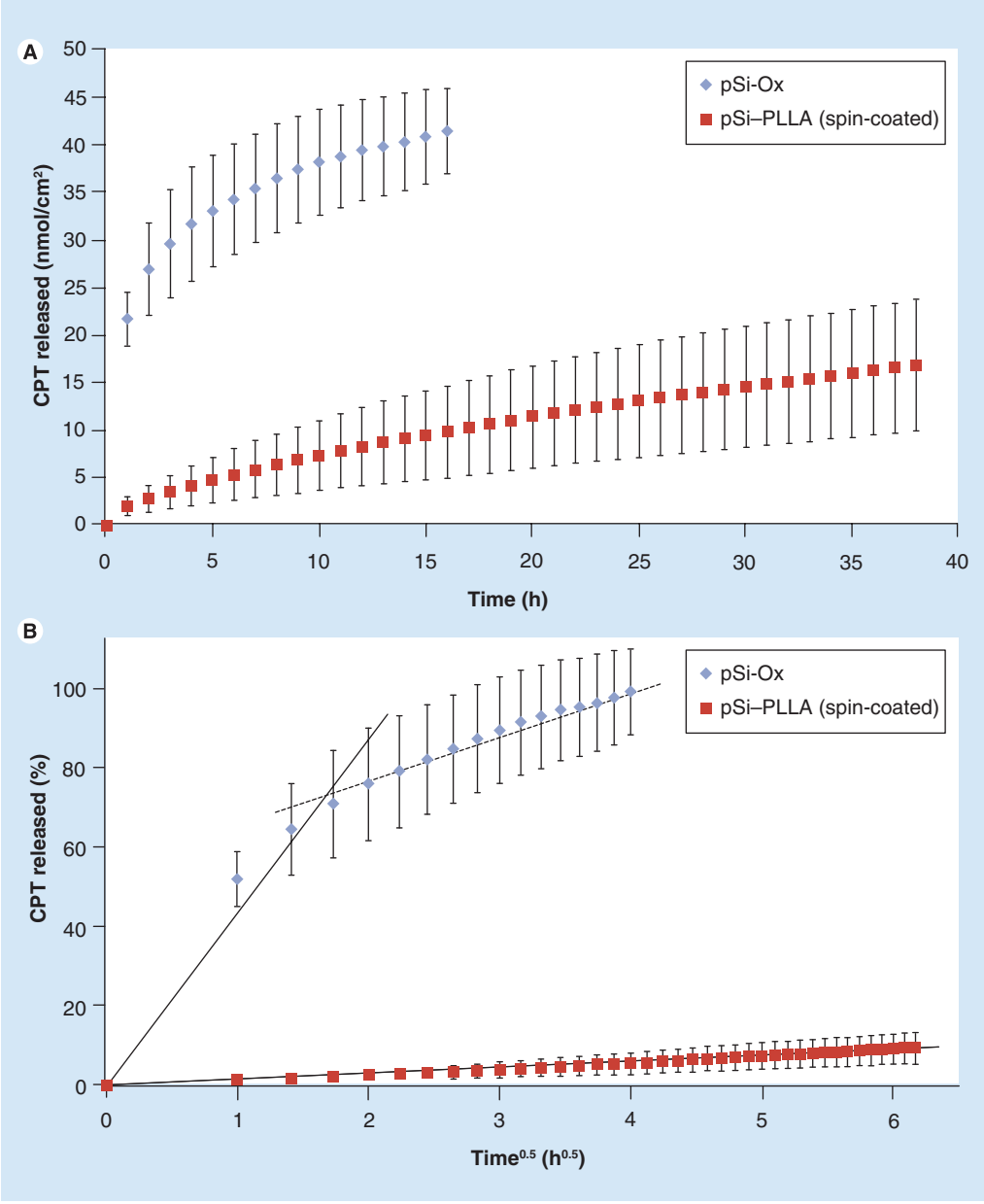

Figure 3. Drug release from porous silicon–poly(L-lactide) (spin-coated) surfaces. (A) Release of CPT from spin-coated pSi–PLLA composite and **(B)** corresponding Higuchi plot of CPT release. CPT: Camptothecin; Ox: Oxidized; PLLA: Poly(L-lactide); pSi: Porous silicon.

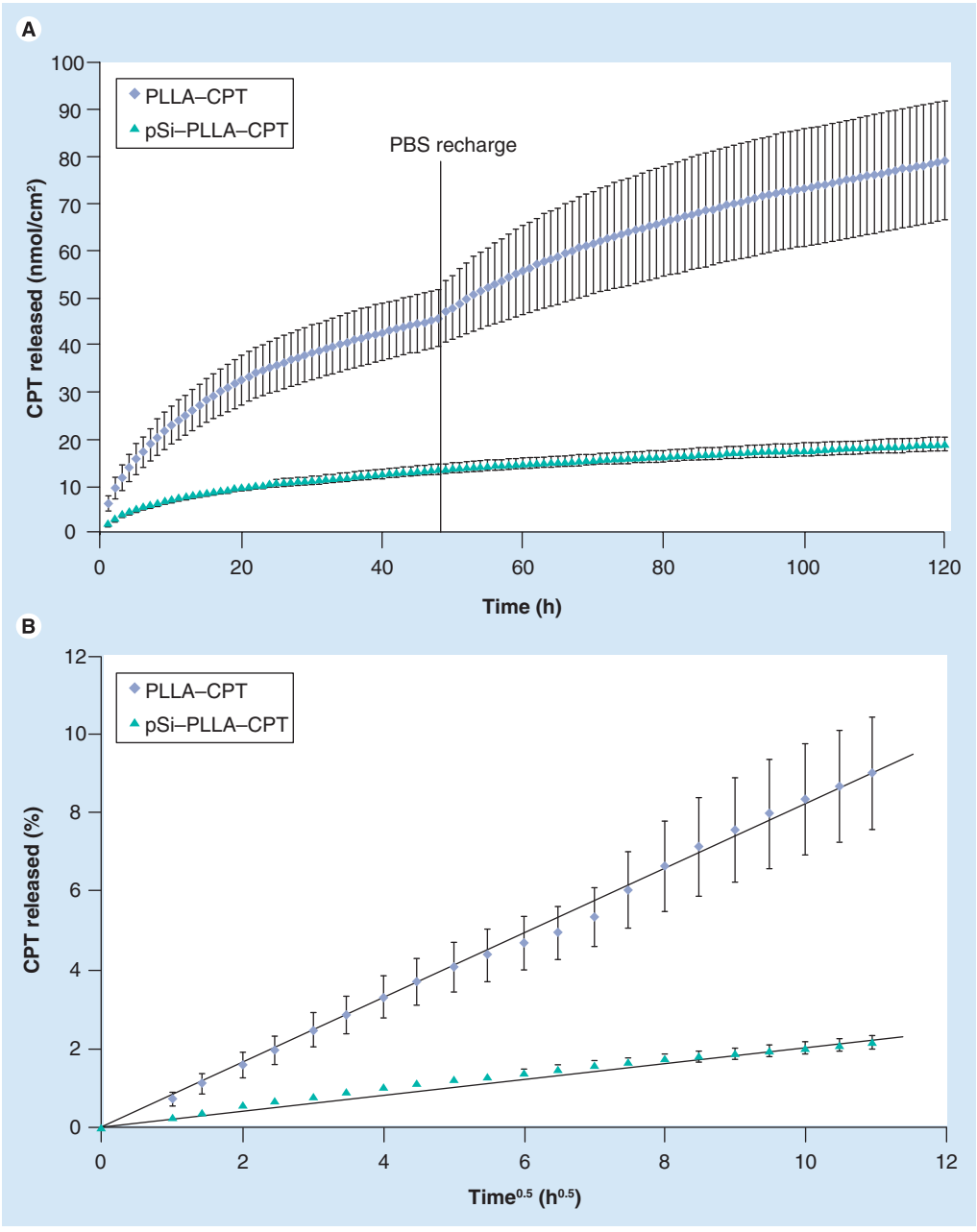

Figure 4. Drug release from poly(L-lactide) monoliths. (A) Release of CPT from PLLA only and pSi–PLLA monoliths and **(B)** corresponding Higuchi plots of CPT release.
CPT: Camptothecin; PBS: Phosphate-buffered saline; PLLA: Poly(L-lactide); pSi: Porous silicon.

at the release end point (~1.4 µM). The absence of photobleaching over the maximal release period of 5 days was confirmed via sampling a standard CPT solution under the same conditions. The CPT fluorescence did not change over that time period.

To gain an idea of the release properties of the generated materials, the drug release profiles were plotted against zero-order, first-order, Higuchi, Hixson–Crowell and Ritger–Peppas models and their R^2 values were compared as is a common practice in the literature [62–68].

Cell culture, staining & imaging

Human lens epithelial cells, SRA 01/04, were seeded in 24-well plates at a density of 1×10^5 cells per well in DMEM containing 10% fetal bovine serum, 100 U/ml penicillin, 100 µg/ml streptomycin and 0.29 mg/ml glutamine (complete medium) and allowed to attach overnight at 37°C and 5% CO_2 in air. pSi films and monoliths were then placed etched side down onto the cells after changing to fresh medium. pSi films were left on the cells for 48 h, while the monoliths were left for 5 days. After incubation,

the pSi films or monoliths were removed and the number of cells was assayed using the CellTiter Aqueous One® assay (Promega, WI, USA) according to the manufacturer's instructions. The cells were then stained as follows: SYTOX® Green Stain (Invitrogen, CA, USA) was diluted 1/5000 in complete medium. The medium was replaced with SYTOX staining solution and incubated at 37°C for 20 min after which time the solution was replaced by Cell Mask Orange (Invitrogen) diluted to 1/2000 in complete medium and incubated for 3 min. Cells were then washed with PBS pH 7.4 and fixed for 10 min in 3.7% formalin in PBS. The cells were washed twice with PBS, incubated in 2 µM Hoechst 33342 (Sigma, MO, USA) in PBS for 5 min, followed by washing twice with PBS. All samples were stored in buffered glycerol.

Samples were imaged on an Olympus IX71 inverted microscope. The cells were counted based on the number of Hoechst dye-stained nuclei present in each image. The number of cells found in the untreated wells was used as the 100% mark and all further cell counts were reported relative to this. Cells exposed to medium containing 500 nM CPT were analyzed simultaneously with the composite materials. An analysis of variance test was performed on the cell count data to test for statistical differences (given as p-values). The level of significance was set at $\alpha = 0.05$ (i.e., if $p < 0.05$, samples were determined to be statistically significantly). All data analysis was performed with PASW Statistics 18 software (SPSS Inc., IL, USA).

(3-(4,5-dimethylthiazol-2-yl)-5-(3-carboxymethoxyphenyl)-2-(4-sulfophenyl)-2H-tetrazolium) assay

After the required incubation time (48 h for films or 5 days for monoliths) the pSi film or monolith was removed from the cell culture well and the medium was replaced (1 ml). Subsequently, 100 µl of (3-(4,5-dimethylthiazol-2-yl)-5-(3-carboxymethoxyphenyl)-2-(4-sulfophenyl)-2H-tetrazolium) (MTS; CellTiter One reagent, Promega) was added and the cells were incubated at 37°C for 2 h, after which time 100 µl aliquots were removed and analyzed at 490 nm on a VERSAmax™ tunable microplate reader with Softmax Pro 4.8 software (Molecular Devices, CA, USA).

Results & discussion

pSi characterization

Gravimetric analysis of the pSi films, as outlined by Canhan [25], was used to determine the porosity of the films and gave values of approximately 82%. A similar porosity of 75% was obtained by effective medium calculations from interferometric reflectance spectroscopy measurements. Cross-sectional analysis of the films by means of SEM analysis gave a film thickness of approximately 7 µm (Figure 5A) and topographical analysis by AFM revealed a pore diameter of 8–12 nm (Figure 5B).

The etched pSi films used to produce pSi microparticles for preparation of pSi–PLLA monoliths had a porosity of 70 and 79% by gravimetry and effective medium calculations, respectively. SEM analysis of the microparticles showed an assortment of slab-like structures that varied in

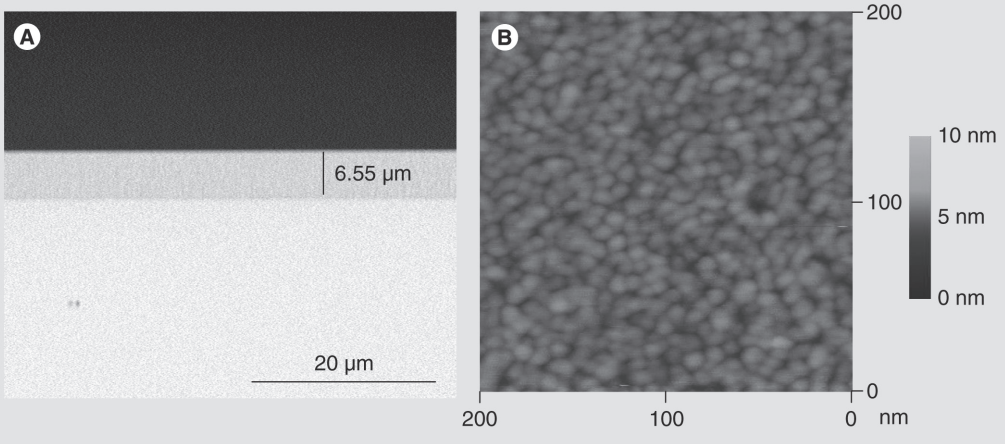

Figure 5. Scanning electron microscopy and atomic force microscopy characterization of porous silicon. (A) Scanning electron microscopy micrograph showing the thickness of the porous silicon films and **(B)** tapping mode atomic force microscopy image of a porous silicon film used for grafting and spin coating of poly(L-lactide).
Color figure can be found online at www.futuremedicine.com/doi/full/10.2217/nnm.11.176

size with an average particle size of 85 ± 45 µm (FIGURE 6A). Close inspection of the particles via SEM revealed that some of the larger particles had a tendency to curl up slightly (FIGURE 6B) and a thickness of around 10 µm (FIGURE 6C). AFM imaging revealed a pore size range of 12–16 nm (FIGURE 6D).

Characterization of composite materials

The composite materials prepared for this work were characterized via IR spectroscopy, AFM, SEM and contact angle measurements. Characterization of the pSi–PLLA (grafted) composites is also described in our earlier work [38].

Chemical analysis of the composite materials via IR spectroscopy confirmed the presence of a PLLA layer. FIGURE 7 shows typical transmission IR spectra of each of the composite materials. In order to collect IR data, the composite materials were produced on p^+ type (resistivity 3–6 Ωcm, <1–0–0>) pSi to allow for transmission IR to be performed. The spectra of ozone-pSi-Ox (FIGURE 7) showed a strong and broad peak centered at 1045 cm^{-1} due to asymmetric stretching vibrations of Si–O-Si surface bridging groups [69]. Other than a weak and broad peak centered around 3415 cm^{-1} attributed to the presence of surface silanol groups, the spectrum lacked other peaks of significance. After the grafting of PLLA from pSi-Ox (pSi-Ox–PLLA; grafted) (FIGURE 7), the IR spectra still showed the strong characteristic peak at 1045 cm^{-1} and a new peak at 1349 cm^{-1}, which was attributed to the methyl-bending vibrations of the PLLA. The broad band centered at 3400 cm^{-1} increased in intensity and was attributed to the free hydroxyl groups from the polymer termini as well as surface silanol groups. The peak at 1444 cm^{-1} was assigned to the asymmetric CH_3 deformation mode and the dual peak at 2920 and 2965 cm^{-1} corresponds to C-H stretching vibrations of the PLLA. Perhaps most notable was the appearance of a conspicuous new peak occurring at 1725 cm^{-1} attributed to the C=O stretching mode of the PLLA, confirming the presence of a PLLA on the surface.

Similar IR spectra were obtained after PLLA grafting from pSi functionalized with HEAPS and PEGS [38]. The spectrum of PLLA spin-coated on ozone-pSi-Ox also showed the same characteristic set of peaks as the grafted samples

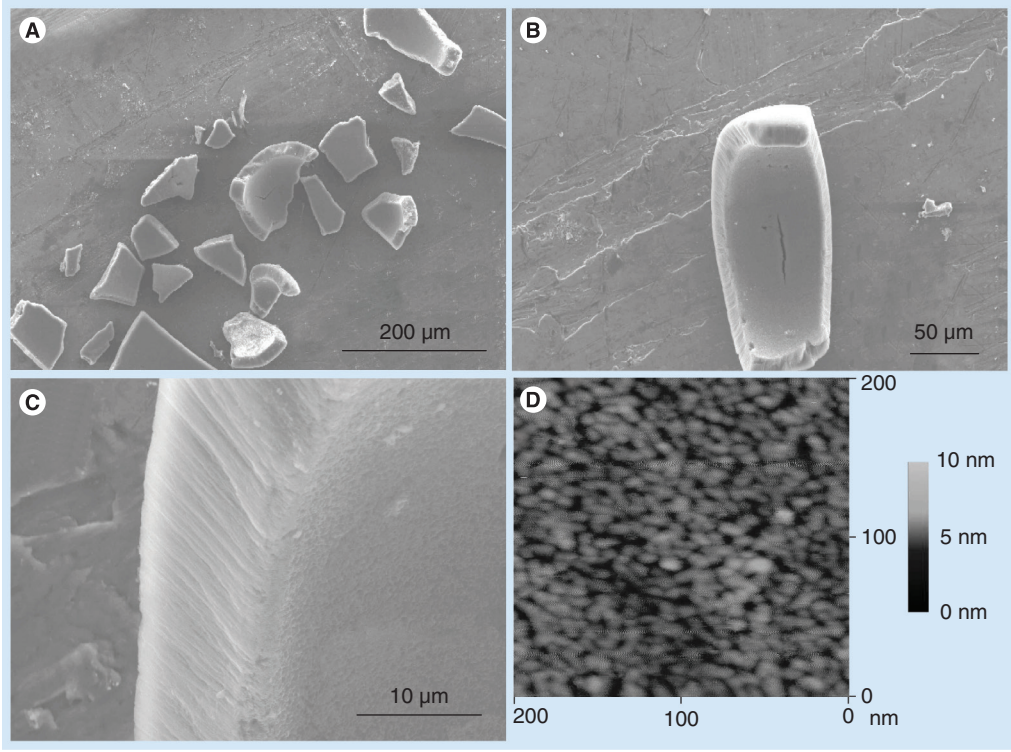

Figure 6. Scanning electron microscopy and atomic force microscopy images of porous silicon microparticles. (A) Scanning electron microscopy images of representative porous silicon microparticles. **(B)** A single microparticle. **(C)** Edge view of a single microparticle showing the layer thickness and the porous nature of the particle and **(D)** tapping mode atomic force microscopy image of a porous silicon film used to make porous silicon microparticles before electropolishing. Color figure can be found online at www.futuremedicine.com/doi/full/10.2217/nnm.11.176

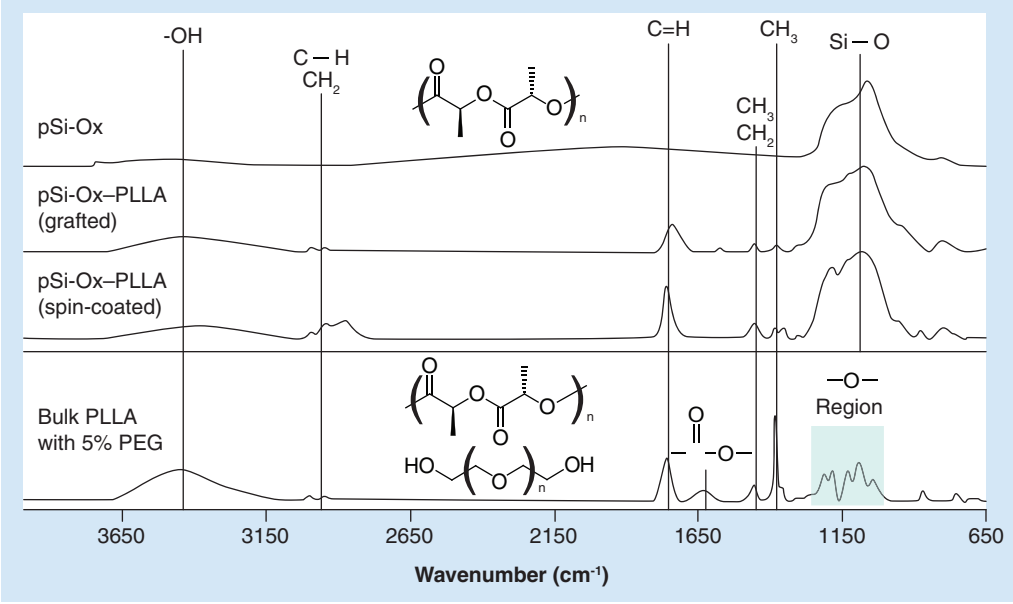

Figure 7. Comparison of infrared spectra of the poly(L-lactide) composite materials.
Ox: Oxidized; PEG: Polyethylene glycol; PLLA: Poly(L-lactide); pSi: Porous silicon.

but with a greater intensity than seen for the latter (pSi-Ox–PLLA; spin-coated) (Figure 7). The spectra of bulk PLLA used to produce the monolith materials (bulk PLLA with 5% w/w PEG 6000; average molecular weight 6000–7500 g/mol) (Figure 7) featured similar spectral peaks as the pSi–PLLA (grafted) and pSi–PLLA (spin-coated) composites, with the exception of the region from 1000–1300 cm^{-1} (highlighted box in Figure 7). The C-O-C stretching vibrations and the C-H rocking modes observed for bulk PLLA in that region are overshadowed by the Si-O peak in the composite materials [70].

The PLLA by-product formed in solution during the surface-initiated ring-opening polymerization reaction was analyzed via size exclusion chromatography and found to have a molecular weight of approximately 9434 g/mol with a polydispersity of 1.13. This polydispersity value is indicative of a well-controlled polymerization reaction [71,72]. The determined average molecular weight also fits well with estimates from our previous work, which used TGA to estimate the average molecular weight of the surface-bound polymer produced on the pSi film at approximately 10,000 g/mol [38].

In terms of surface morphology, our earlier AFM study of the pSi–PLLA (grafted) pSi films showed the presence of PLLA nanobrushes [38]. The presence of the PLLA layer after spin

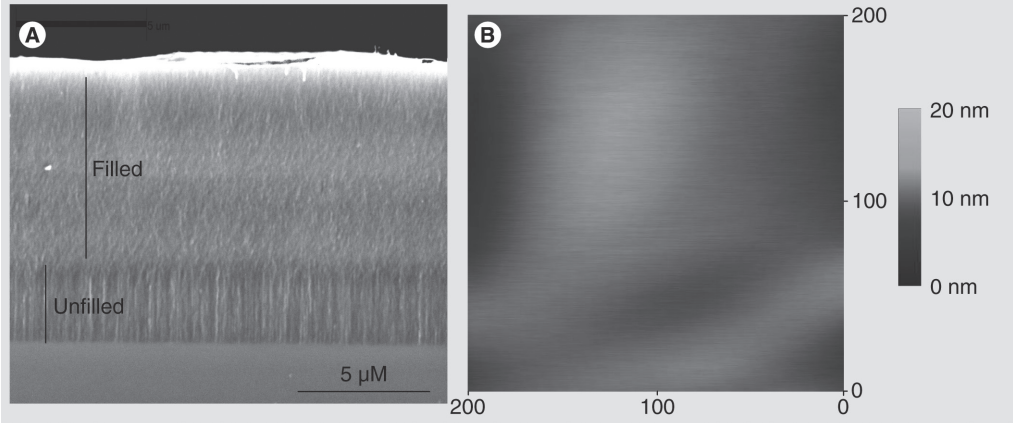

Figure 8. Scanning electron microscopy and atomic force microscopy characterization of spin-coated composite materials. (A) Cross-sectional scanning electron microscopy micrograph of an oxidized porous silicon–poly(L-lactide; spin-coated) and **(B)** tapping mode atomic force microscopy image of oxidized porous silicon–poly(L-lactide; spin-coated).
Color figure can be found online at www.futuremedicine.com/doi/full/10.2217/nnm.11.176

coating and melting of the PLLA on pSi films was confirmed via SEM (Figure 8A). SEM revealed a 4.2-µm thick layer on top of the pSi and that 3.6 µm of this PLLA layer had penetrated into the pSi pore structure. This left the lower 3.0 µm of the pSi unfilled. The extent of penetration could possibly be increased by longer melting times or by physically forcing the molten PLLA into the pores. On the other hand, the presence of a pore volume not filled with PLLA presents opportunities for high drug loading. In this case, the PLLA would act as a plug, closing off the pores. Indeed, AFM analysis of the pSi–PLLA (spin-coated) (Figure 8B) shows that the pores have been totally occluded by polymer, in contrast to the pSi-Ox (Figure 5B) and to pSi–PLLA (grafted) [38]. Due to solubility issues, the molecular weight of PLLA used for the spin coating and monolith production was determined from TGA measurements by using the published relationship between decomposition temperature and molecular weight [73]. We obtained a molecular weight of around 25,000 g/mol.

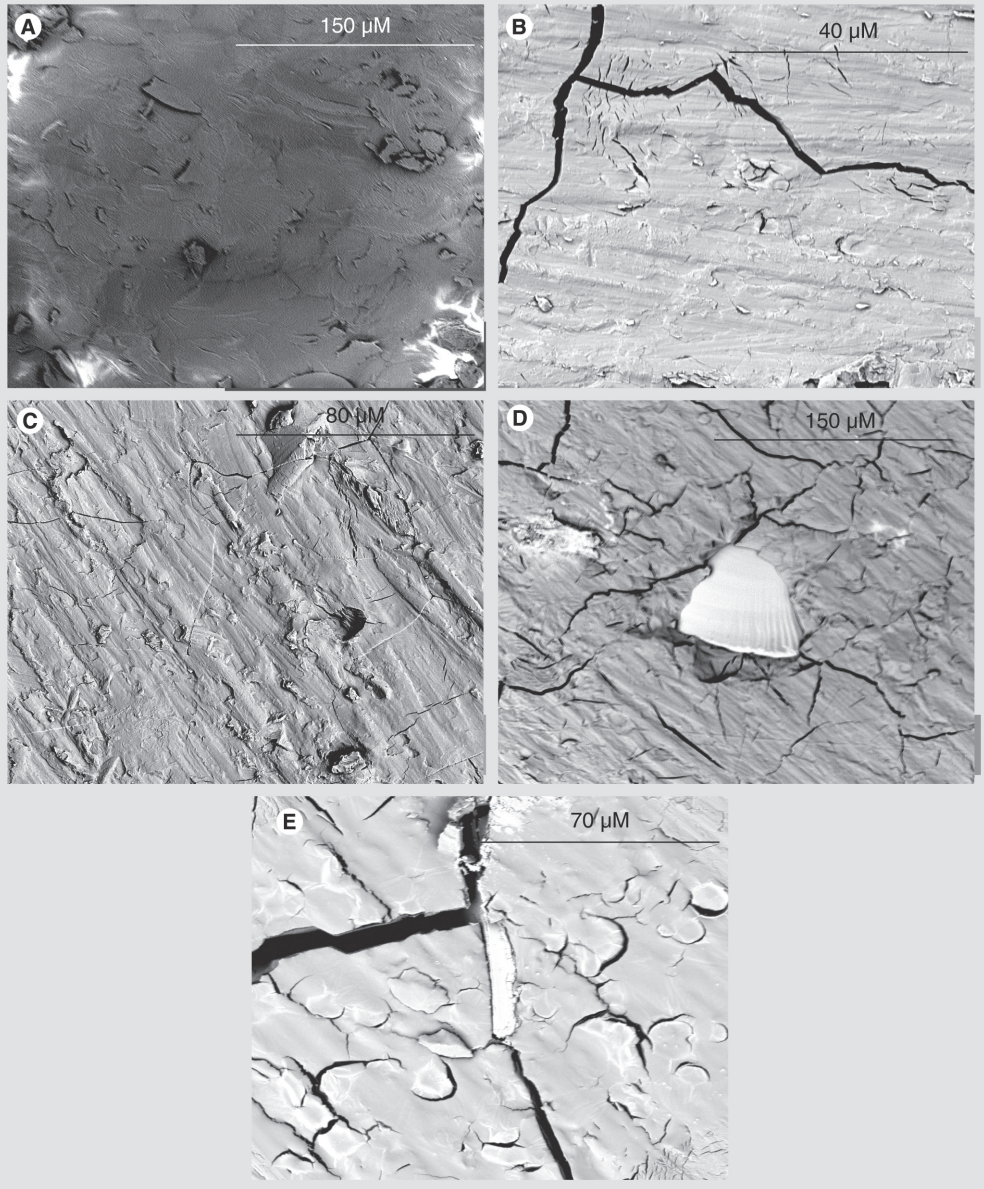

Figure 9. Scanning electron microscopy analysis of degradation occurring in the poly(L-lactide) monolith structures. Scanning electron microscopy micrographs of poly(L-lactide)–camptothecin monolith surfaces **(A)** before degradation in phosphate-buffered saline and **(B)** after degradation for 1 month, and scanning electron microscopy micrographs of monolithic porous silicon–poly(L-lactide)–camptothecin composites **(C)** before degradation and **(D & E)** after 1 month of degradation in phosphate-buffered saline.

Table 1. Camptothecin loading of composite materials and their estimated degradation times.

Material type	Loading (nmol of CPT per cm^2)	Degradation time
pSi–PLLA (grafted)	37.0 6.4	<24 h
pSi–PLLA (spin-coated)	178.7 ± 9.6	Weeks
pSi–PLLA monolith	11.5 ± 0.1 nmol/mg	Months

CPT: Camptothecin; PLLA: Poly(L-lactide); pSi: Porous silicon.

We also prepared monolithic materials by melt casting bulk polymerized PLLA with and without pSi microparticles in an aluminum mould. The PLLA monoliths without pSi microparticles were characterized by SEM (Figure 9A). They were an opaque white and their surface appeared quite smooth in the SEM image. The monolithic pSi–PLLA composites showed a similar topography by SEM (Figure 9C) although they appeared light brown in color. We investigated the stability of the monoliths in PBS under the same conditions used for the release experiments. After 1 month of shaking incubation at 37°C in nonsterile PBS (pH 7.4), washing with water and drying, the outer surface of the monoliths had cracked extensively (Figures 9B, D & E). Macroscopically, the entire structure had become more opaque. This was observed both in the absence and presence of pSi microparticles. These results indicate that significant PLLA degradation has occurred in PBS over this time frame. We also found evidence of degradation of the pSi microparticles, as the pSi–PLLA monoliths became lighter in color. In some cases, individual microparticles became exposed during the incubation in PBS (Figures 9D & E). Monolith materials kept in PBS solution for a period of 3 months lost all structural integrity (see Table 1 for the estimated degradation times of all three types of composite material).

Surface wettability is an important parameter for biodegradable materials. We determined the WCA for all of the composite materials produced in this study (Table 2), including the three different grafted composites. It should be noted that the WCA is influenced both by the surface chemistry and the topography of the material, and in some cases both parameters change between the composites.

Sessile drop WCA measurements qualitatively showed similar wettability for all the grafted composites. As shown in Table 2, upon surface-initiated polymerization of PLLA, a WCA increase of approximately 40° (14–54°) was observed. Approximately 30° higher contact angles were subsequently measured on pSi–PLLA (spin-coated). This difference in wettability was possibly caused by the thin coating on the grafted composites still exposing some surface chemistry of the pSi or the difference in topography between the grafted and the spin-coated surfaces (Figure 8B) [38]. The monolithic composite and bulk polymerized PLLA gave very similar WCA to the spin-coated composites.

CPT loading & release

Each composite material was loaded with the cytotoxic drug CPT, a relatively water-insoluble small-molecule alkaloid drug [74] first isolated from the stem wood of *Camptotheca acuminata* by Wall *et al.* [75]. CPT is an antineoplastic agent that exerts its anti-tumor effect by the inhibition of the nuclear enzyme topoisomerase I [76]. Although CPT shows a broad spectrum of activity towards many cancers it has yet to be used *in vivo* due to its poor solubility and rapid hydrolysis to a ring-open carboxylate form with lower pharmacological activity [61]. As we are interested in drug delivery to the eye, CPT was selected as a model drug because of its rapid cytotoxic profile and the ease with which it can be quantified. It has a similar molecular mass to the DNA cross-linking agent mitomycin C, which is administered topically to the eye after some glaucoma-filtering surgery [77]. Mitomycin C is also cytotoxic for mammalian cells, but is more difficult to quantify accurately than CPT.

Table 2. Water contact angle of porous silicon–poly(L-lactide) composite materials and bulk polymerized poly(L-lactide) (n = 6).

Material	WCA ± standard deviation
pSi-Ox	14.0 ± 2.0
pSi-Ox–PLLA (grafted)	54.0 ± 5.4
pSi–HEAPS–PLLA (grafted)	54.1 ± 8.4
pSi–PEGS–PLLA (grafted)	49.4 ± 3.7
pSi–PLLA (spin-coated)	80.3 ± 2.6
pSi–PLLA (monolith)	78.2 ± 3.3
Bulk polymerized PLLA [91]	79.0 ± 3.0

HEAPS: N-*(hydroxyethyl)-3-aminopropyl trimethoxysilane; Ox: Oxidized;*
PEGS: N-*(triethoxysilylpropyl)*-O-*polyethylene oxide urethane; PLLA: Poly(L-lactide); pSi: Porous silicon; WCA: Water contact angle.*

The loading was performed by placing the pSi films or microparticles into a solution of CPT in DMF before drying under vacuum, or in the case of the monoliths by solid–solid mixing, as described in the section 'Production and loading of pSi–PLLA monoliths'. The final loading values are displayed in Table 1. Release experiments with CPT were performed in PBS, hence we expected the CPT to remain in its bioactive (closed ring) form. The total CPT loadings for each of the surface-grafted materials was calculated from the average of the final fluorimetry reading of each release curve, while the loadings for the spin-coated and monolithic materials were calculated gravimetrically. These total loading values (Table 1) were then used to convert the released amounts of CPT (determined via fluorimetry) into percentage of total CPT released. In the case of the films, the loaded amount was normalized to the film's surface area, while loading was normalized to total weight in the case of the monoliths.

The release of CPT from all of the grafted pSi–PLLA composites (Figure 2A & Table 3) showed a substantial burst release within the first 1 h before a transition release of approximately 5 h, in which the release rate slows and starts to plateau into a slow linear release phase, lasting approximately 10 h. This is due to the incomplete coating of the pores allowing the CPT to diffuse quickly from the pSi network, possibly also due to the high wettability of those materials. Release from the PLLA grafted composites was only marginally slower than from unpolymerized, CPT-loaded pSi films (denoted pSi-Ox), which showed a fast burst release of 51.9% of loaded CPT over the first 1 h. The pSi–PEGS–PLLA surface was able to release the largest percentage of CPT in a linear fashion (21.4% of the total CPT loading). The transition release, which is neither a burst release nor a linear release, was typically responsible for the release of approximately 30–50% of the total CPT loading (Table 3).

pSi is susceptible to hydrolytic degradation and the thin PLLA layer provides relatively little protection to the pSi scaffold [7,78]. Indeed, these grafted films completely dissolved within the 15-h time frame of the release curves and, hence, released their full CPT payload (approximately 37.0 nmol of CPT per cm^2 of pSi on average for the four different composite materials). These materials are clearly unsuitable for long-term controlled drug release applications. However, they are adequate for short-term release, such as that required for the delivery of an antibiotic.

The release of CPT from the spin-coated pSi–PLLA composites (Figure 3 & Table 3) into PBS showed a burst release of 0.7% of the loaded material at a rate of 5.1 nmol/cm^2.h within the first 30 min before a linear release phase over approximately 38 h (8% of total loading, 0.4 nmol/cm^2.h). The release from these materials did not show a pronounced transition phase as observed for the pSi–PLLA (grafted) composites. These materials were not as susceptible to hydrolytic degradation over this time frame since the thicker PLLA layer protects the pSi scaffold. Indeed, it took several weeks before pSi degradation was visible.

Considering the linear release rate, these materials could potentially release CPT for up to 400 h or roughly 6.5 days and, hence, possess attractive release properties. It is straightforward

Table 3. Comparison of camptothecin release rates for the different types of composite materials and their corresponding R^2 values.

Material	Burst rate (nmol/cm^2.h)	Burst release (%)	Linear rate (nmol/cm^2.h)	Linear release (%)	Linearity (R^2)	Transition release (%)	Final release (%)	Approximate 100% release time
pSi-Ox†	21.6	51.9	0.7	16.6	0.970	31.6	100.0	15–20 h
pSi-Ox–PLLA (grafted)†	13.8	36.3	0.6	13.0	0.950	50.7	100.0	15–20 h
pSi–HEAPS–PLLA (grafted)†	13.4	48.2	0.4	12.2	0.982	39.7	100.0	15–20 h
pSi–PEGS–PLLA (grafted)†	14.7	36.0	1.0	21.4	0.983	42.5	100.0	15–20 h
pSi–PLLA (spin-coated)‡	5.1	0.7	0.4	8.0	0.984	0.4	9.1	400 h
PLLA–CPT (monolith)§	7.6	1.1	0.7	5.3	0.981	2.6	9.0	50 days
pSi–PLLA–CPT (monolith)§	2.6	0.4	0.1	1.0	0.979	0.8	2.2	232 days

†*Burst release calculated over the first 1 h, linear release and R^2 values calculated from 6 h to release end.*
‡*Burst release calculated over the first 0.5 h, linear release and R^2 values calculated from 1 to 38 h.*
§*Burst release calculated over the first 2 h, linear release and R^2 values calculated from 20 to 120 h.*
CPT: Camptothecin; HEAPS: N*-(hydroxyethyl)-3-aminopropyl trimethoxysilane; Ox: Oxidized; PEGS:* N*-(triethoxysilylpropyl)-*O*-polyethylene oxide urethane; PLLA: Poly(*L*-lactide); pSi: Porous silicon.*

to generate pSi membranes spin-coated with PLLA, rather than films, to create fully biodegradable implantable drug release materials. Once the drug payload has been completely released, there are clear advantages to the composite material degrading in its entirety.

We next compared CPT release from monoliths with and without pSi microparticles (Figure 4 & Table 3). We conjectured that the release of CPT from pSi microparticles embedded within the PLLA structure would be slower than CPT release from PLLA directly, assuming equivalent amounts of CPT are loaded. The PLLA-only monoliths were loaded with solid CPT dispersed in the PLLA melt (PLLA–CPT), while the pSi–PLLA–CPT monolith was generated by the addition of pSi microparticles previously loaded with CPT. The release curves for the first 2 days (Figure 4A) illustrate a burst release phase of 1.1 and 0.4% CPT release for the PLLA–CPT and pSi–PLLA–CPT monoliths, respectively, before reaching a prolonged linear release phase. Once this linear release phase was reached, the monoliths were taken out and washed before being placed back into release buffer and monitored (PBS recharge mark Figure 4A). Monolith materials demonstrated linear release for 5 days (Figure 4A). Only a small transition release was observed between the burst and linear release phases (Table 3). Over the period of linear release, the CPT release rate from the PLLA–CPT monoliths (~0.7 nmol/cm^2.h) was higher when compared with pSi–PLLA (spin-coated) (~0.4 nmol/cm^2.h). However, the pSi–PLLA–CPT monoliths gave a linear release rate of only 0.2 nmol/cm^2.h). The difference between the two monoliths may be the result of the CPT being trapped into the pore network of the pSi particles, which are, in turn, encapsulated within the PLLA monolith.

Given that both monoliths had approximately the same maximum loading of 878.4 nmol of CPT per monolith and the total release percentage of CPT from the PLLA–CPT and pSi–PLLA–CPT monoliths (over 5 days) was 9.0 and 2.2%, respectively, we can conclude that the preloading of CPT into the pSi before monolith production resulted in a substantially slower release profile. Extrapolating the release data over longer release periods, PLLA–CPT composites should theoretically be able to release CPT for 50 days, while the pSi–PLLA–CPT monolith could release for over 200 days, four-times longer. It is important to note that PLLA is susceptible to hydrolytic degradation and, as we have shown by SEM, this effect will alter the structure of the monoliths over several weeks, which in turn may affect the release rate at extended time periods. It is interesting to note that the pSi microparticles were still intact inside the PLLA monoliths even after 1 month of incubation at 37°C as the SEM images in Figures 9D & E show. While the pH of the bulk solution remained at pH 7.4, it is possible that the local pH in the monolith was acidic due to the degrading PLLA, which would stabilize the pSi microparticles.

When comparing the release of drugs from these materials to a release model, a range of physical characteristics need to be taken into consideration. These include water diffusion into the matrix, drug diffusion out of the matrix, polymer swelling, polymer dissolution, pSi dissolution, porosity and changing matrix dimensions. We have fitted the release data to the common release models applicable to our materials (Table 4) [79–84].

The data shown in Table 4 reveal that the zero-order and Hixson–Crowell models were not suitable models for this set of release data. The latter model describes the drug release by dissolution and changes in surface area and diameter of the particles or tablets [82]. For the grafted thin films, the best fit was in fact the first-order model, which revealed quite high R^2 values (above 0.948). The

Table 4. Comparison of R^2 values of fitting camptothecin release to different release models.

Material	Zero order	First order	Higuchi	Hixson–Crowell	Ritger–Peppas	n
pSi-Ox	0.643	0.952	0.861	0.334	–	–
pSi-Ox–PLLA (grafted)	0.672	0.975	0.886	0.383	–	–
pSi–HEAPS–PLLA (grafted)	0.624	0.948	0.853	0.340	–	–
pSi–PEGS–PLLA (grafted)	0.776	0.954	0.950	0.429	0.982	0.44
pSi–PLLA (spin-coated)	0.973	0.977	0.994	0.704	0.998	0.58
PLLA–CPT (monolith)	0.962	0.966	0.995	0.754	0.996	0.53
pSi–PLLA–CPT (monolith)	0.901	0.903	0.988	0.627	0.993	0.44

–: Model could not be fitted to data as the release was too fast; CPT: Camptothecin; HEAPS: N-*(hydroxyethyl)-3-aminopropyl trimethoxysilane; Ox: Oxidized; PEGS:* N-*(triethoxysilylpropyl)-*O*-polyethylene oxide urethane; PLLA: Poly(*L*-lactide); pSi: Porous silicon.*

Higuchi plot fits the release from the pSi–PLLA (grafted) samples reasonably well and also gives very good fits for the monoliths and for pSi–PLLA (spin-coated). The Higuchi model is an empirical model commonly used to describe the release kinetics of drugs from insoluble porous materials [80,81]. It is well established and commonly used for modeling drug release from matrix systems [81,85,86]. The model is based on a square root of a time-dependent process of Fickian diffusion.

$$Q_t = k_H t_{½}$$

In this model, the plot of percentage drug released (Qt) versus the square root of time should be linear for a purely diffusion controlled process with the slope of the plot equal to the Higuchi release rate constant k_H [87]. Deviations from linearity indicate that the release is not purely diffusion controlled, and may be influenced by other factors, such as the degradation of the matrix material.

All of the grafted pSi–PLLA composites showed a two-phase release in the Higuchi plot and there are quite clearly two different release rates before and after 4 h (Figure 2B). This was attributed to the degradation of the these materials over the time course of the release and, hence, the process was no longer only diffusion controlled as the composite dissolution will assist the release of CPT [87]. The Higuchi plot of CPT release from the spin-coated composite material was linear (R^2 = 0.994) confirming the diffusion-based release in these more stable composite materials. Drug release from the monolithic materials was mainly diffusion controlled over the time frame of 5 days based on the Higuchi plots (Figure 4B) (R^2 = 0.995 for the PLLA-only monolith and R^2 = 0.988 for the pSi–PLLA monolith).

The Ritger–Peppas model also fit the data well. This model (also known as Korsmeyer–Peppas) is used to fit drug release from polymeric thin films, cylinders and spheres [88]. This model can be applied to any system to gain an idea of the apparent overall release phenomenon regardless of the specific mechanisms of release actually occurring [88]. The Ritger–Peppas model is limited to the first 60% of a drug release curve only; diffusion must be 1D (aspect ratio is at least 10:1) and the drug diffusion coefficient must be concentration independent. These conditions are met for most composites in this study. For the grafted samples, with the exception of pSi–PEGS–PLLA, the release data could not be fitted to this model since release was too fast to allow for more then two data points to be plotted below the 60% release limit. The Ritger–Peppas equation is shown below [83,84].

$$\frac{M_t}{M} = K_m t^n$$

where M_t is the amount of drug released at time (t), M is the total amount of drug in dosage form, K_m is the kinetic constant and n is the release exponent. The n exponent is estimated from the slope of $\log_{(Mt/M)}$ versus $\log_{time}$. Values of $n < 0.5$ indicate Fickian diffusion (case 1) and values of $0.5 < n < 1.0$ indicate non-Fickian (anomalous) diffusion [83,84,89]. When using the Ritger–Peppas equation $n < 0.5$ is only possible when porous systems are involved. In these cases, the release mechanism is a combination of diffusion through the swollen matrix polymer and diffusion through the water-filled pores of the porous material [89].

The n-values from the Ritger–Peppas model differ for the composite materials used here. pSi–PLLA (spin-coated) shows an n-value of 0.58 (Table 4), indicating that this material is being released via a combination of Fickian and non-Fickian diffusion. The same is seen for the PLLA–CPT monolith. However, with pSi–PLLA monoliths, the release seems to be by Fickian diffusion. This indicates that the release can be controlled from these composite materials by simply varying the formulation of the composite materials.

Cell cytotoxicity

The CPT released from the pSi–PLLA composite materials was expected to show cytotoxic effects on human lens epithelial cells (SRA cell line), a relevant cell line for *in vitro* testing of drug release to the anterior segment of the eye.

Fluorescence microscopy analysis of the SRA cells in Figure 10 revealed that untreated cells appeared densely packed after the incubation period (Figure 10A), while exposure to 500 nM CPT (positive control) significantly reduced the number of cells remaining adherent (Figure 10B). The CPT concentration used in the positive control (500 nM) is approximately 71.5% of the IC_{50} value of 700 nM found by Peel *et al.* [90]. These images also reveal that the CPT-exposed cells were notably larger than their untreated counterparts, a trend that was also observed for the CPT-loaded composites (Figures 10C–E), which showed very few cells with larger cytoplasms and multiple nuclei, clear signs of CPT-induced DNA damage.

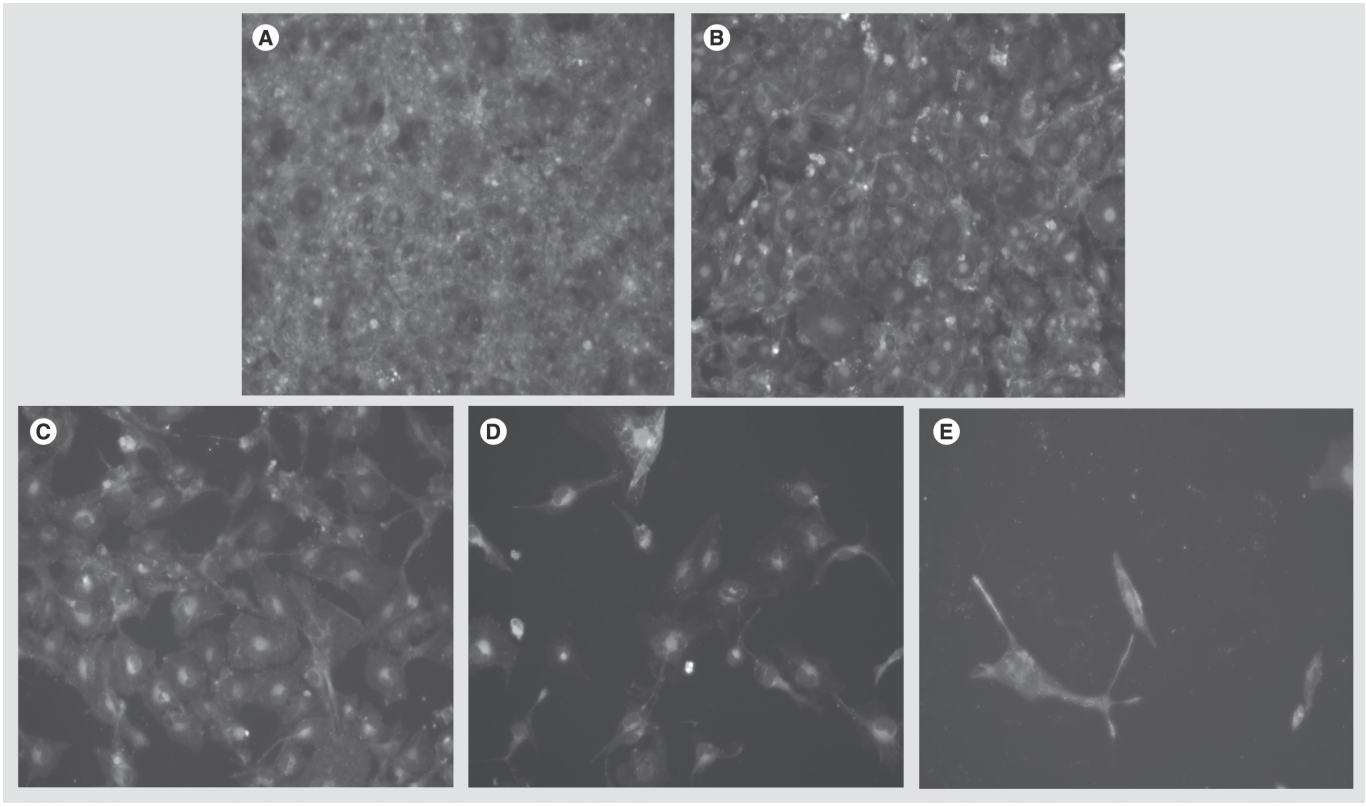

Figure 10. Fluorescence microscopy images of SRA cells stained with SYTOX® Green, Cell Mask™ Orange and Hoechst® 33342 after incubation on camptothecin-loaded composite materials. (A) Untreated (2 days), **(B)** 500 nM camptothecin in complete medium (2 days), **(C)** grafted porous silicon–poly(L-lactide) (2 days), **(D)** spin-coated porous silicon–poly(L-lactide) (2 days) and **(E)** monolith materials (5 days). All images were taken with 10× magnification.

First, counts of cells adherent to tissue culture plates were performed after 48-h incubation of SRA cells in contact with the grafted and spin-coated composite materials, and after 5 days for the monoliths. The extended incubation with the monoliths was justified by taking into account the substantially slower drug release rate from this material. Cell counts in the sample wells were normalized to cell counts from a standard untreated culture with all cells seeded at the same density (Figure 10). Cells in contact with 500 nM CPT solution (48 h and 5 days for films and monoliths, respectively) were also counted. Sink conditions were not maintained for cell culture experiments, as increasing the cell culture volume above 2 ml in each well of a 24-well plate results in an insufficient surface area:volume ratio to maintain appropriate levels of oxygenation in the medium. Table 5 shows the estimated concentration of CPT in the cell culture medium based on the release curves in Figures 2–4. These are not measured values and are only indicative of the possible concentration in each cell culture well.

We also performed the colorimetric MTS assay using a CellTiter One assay kit (Promega), which quantifies the activity of cellular enzymes that reduce MTS to a formazan dye, giving a purple color. The absorbance can then be related to cell viability. The cell viability after exposure to all composite materials was assayed in this manner and the results from the MTS assay were in close agreement with the cell counts (Figure 11). The 100% control used for the MTS assay was untreated cells grown under the same conditions as those exposed to the CPT-containing materials.

The positive control (500 nM CPT in cell culture medium) effectively induced cell death in the SRA cells and reduced the percentage of cells to approximately 60.6%. The cell count results for the film-based composites (Figure 11) showed that all the CPT-loaded materials caused a significant reduction in the SRA cell numbers when compared with untreated cells ($p \leq 0.007$), a similar reduction was seen for the positive control. This result confirms that the released CPT is still in a bioactive form. CPT-loaded pSi-Ox (pSi-Ox–CPT) showed the greatest reduction in cell numbers, with only 43.5% of cells viable after incubation compared with the negative control. From the release curves, the estimated CPT concentration in culture medium after 2 days for the CPT-loaded pSi-Ox and pSi–PLLA (grafted)

Table 5. Estimated camptothecin release amounts and corresponding cell viability.

Sample	Average estimated CPT concentration in media (μM)	Cell count viability (%)	MTS cell viability (%)
500 nM std (2 days)	0.50	60.6 ± 6.5	63.2 ± 2.3
pSi-Ox only	0.00	97.8 ± 5.1	99.1 ± 2.6
pSi-Ox–CPT	2.78	43.5 ± 10.6	50.8 ± 15.4
pSi–PLLA–CPT (grafted)	2.78	52.5 ± 5.5	59.7 ± 4.4
pSi–PLLA (spin-coated)	0.95	68.1 ± 6.9	70.7 ± 12.3
500 nM std (5 days)	0.50	22.1 ± 3.1	36.3 ± 2.9
PLLA only	0.00	83.6 ± 7.3	83.9 ± 7.4
PLLA–CPT (5 days)	17.54	0.9 ± 0.4	4.2 ± 1.9
pSi–PLLA–CPT (5 days)	4.20	1.3 ± 0.3	0.0 ± 1.8

CPT: Camptothecin; MTS: 3-(4,5-dimethylthiazol-2-yl)-5-(3-carboxymethoxyphenyl)-2-(4-sulfophenyl)-2H-tetrazolium; Ox: Oxidized; PLLA: Poly(L-lactide); pSi: Porous silicon; std: Standard.

films averaged 2.78 μM (Table 5). The spin-coated sample also showed the least reduction with 68.1% of cells compared with the untreated negative control. The estimated CPT concentration in culture medium after 2 days was 0.95 μM, consistent with the expected slower release compared with the grafted samples. When an analysis of variance test was performed on the cell death found with the grafted pSi–PLLA and spin-coated composite materials, no statistically significant

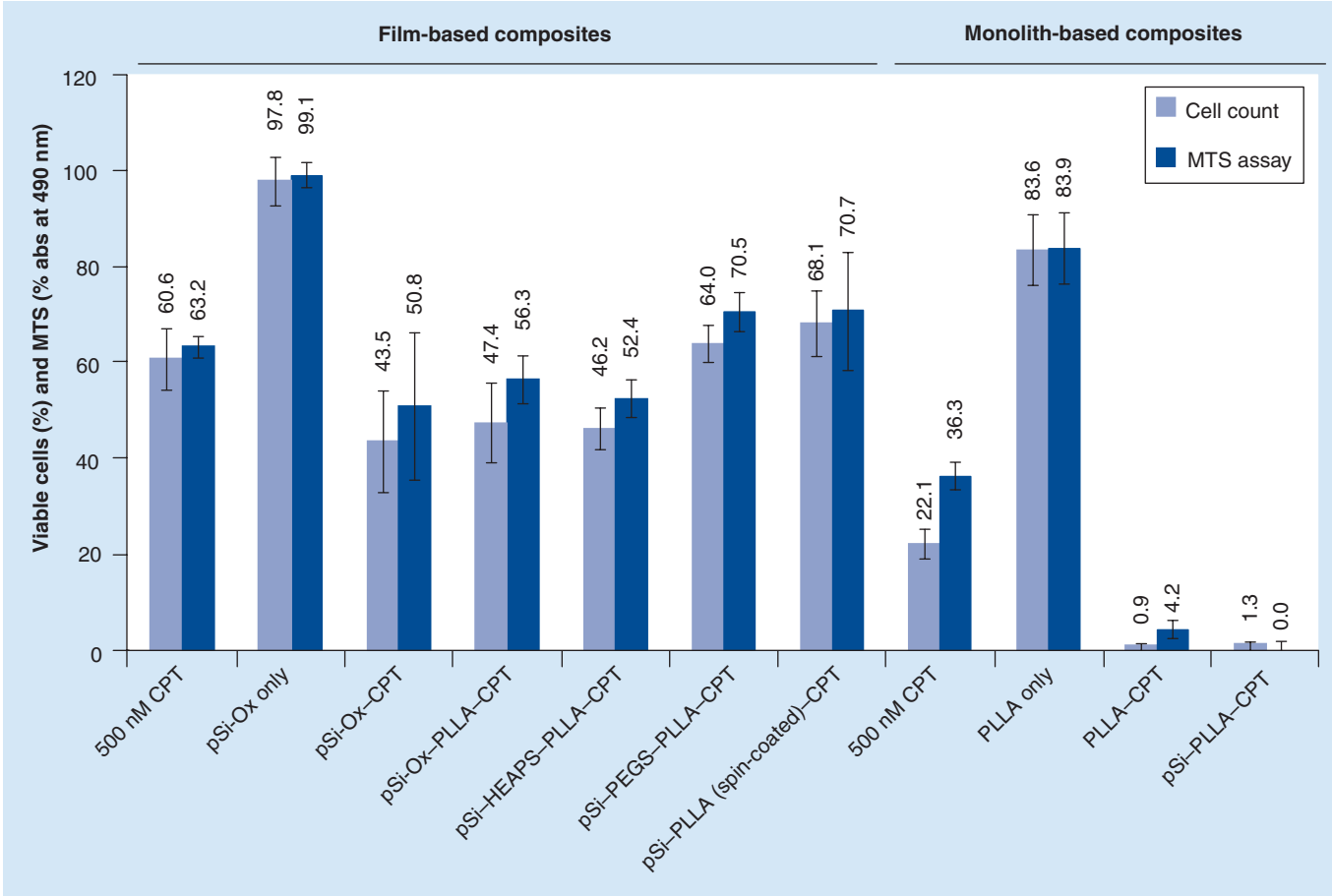

Figure 11. Cell counts, expressed as a percentage of the number of live cells in the average untreated well, for the film (taken after 2 days of incubation) and monolith (taken after 5 days of incubation) based materials.
abs: Absorbance; CPT: Camptothecin; HEAPS: *N*-(hydroxyethyl)-3-aminopropyl trimethoxysilane; MTS: 3-(4,5-dimethylthiazol-2-yl)-5-(3-carboxymethoxyphenyl)-2-(4-sulfophenyl)-2H-tetrazolium; Ox: Oxidized; PEGS: *N*-(triethoxysilylpropyl)-*O*-polyethylene oxide urethane; PLLA: Poly(L-lactide); pSi: Porous silicon.

difference was found. Cell numbers in contact with the non-CPT-loaded pSi-Ox material were essentially unchanged from the controls (97.8%), illustrating that the pSi component of the composite material has only minimally toxic effects on the cells.

The CPT-loaded monoliths (Figure 11) appeared to induce the most effective cell death with less than 5% of cells remaining viable when compared with the negative control after 5 days. The estimated CPT concentration in culture medium for PLLA–CPT after 5 days was 17.54 µM, while for pSi–PLLA–CPT monoliths, the estimated CPT concentration in culture medium was 4.20 µM. The positive control (500 nm CPT in cell culture medium) showed significantly less cellular toxicity due to the much lower concentration of CPT in solution (Table 5). The PLLA monolith without loaded CPT showed a slightly reduced cell count (83.6%) compared with the negative control ($p < 0.001$). However, there was significantly greater cell toxicity with the two CPT-containing monoliths ($p < 0.001$). It is also possible that the presence of the composite materials not loaded with CPT may have caused reduced nutrient flow to the cells by covering the cells during the incubation period and possibly due to some toxicity from the residual $Sn(Oct)_2$ catalyst.

Conclusion

In this article, we described the fabrication of three different architectures of PLLA and nanostructured pSi. These composites are biodegradable and inorganic/organic hybrids. The combination of a pliable polymeric material with a highly porous material, both of which are biodegradable, should be advantageous for applications in localized drug delivery, such as in the treatment of ocular diseases, where flexibility (e.g., for ease of implantation) and high drug payload are desirable attributes. We demonstrated the loading and release of cytotoxic topoisomerase inhibitor CPT, a model cytotoxic drug of a similar size to 5-fluorouracil and mitomycin C, commonly used in glaucoma surgery. The morphology of the composite materials greatly affected the drug release behavior. pSi surfaces grafted with thin films of PLLA by surface-initiated polymerization possessed similar release behavior to pSi lacking the PLLA grafting (pSi-Ox) and were deemed to only be effective for release periods of less than 24 h. These materials also gave rise to a substantial burst release. pSi–PLLA (spin-coated) showed slower CPT release and should sustain release over more than 1 week. The release properties of the spin-coated composites are tunable by varying the thickness and infiltration depth of the PLLA film into the pSi film. This will be the focus of a future study. Monoliths with CPT loaded into pSi microparticles (pSi–PLLA–CPT) showed slower CPT release in comparison with monoliths where CPT was simply mixed directly into the polymer (PLLA–CPT). Monolithic structures are suitable for drug release over time frames of more than 1 month. Our proof-of-principle *in vitro* experiments with human lens epithelial cells suggest that the pSi–PLLA composites may be suitable for localized drug therapy for blinding conditions of the human eye such as uveitis, glaucoma and corneal neovascularization. The loading and release of immunosuppressants and antiglaucoma drugs will be the subject of a future study.

Future perspective

The Si–polymer hybrid materials described here have demonstrated potential for the controlled delivery of small molecular drugs. In the near future, improvements in surface modification with smart polymers could allow for site-specific targeting and improved composite materials that are capable of better protecting therapeutic agents *in vivo* while also improving the release properties. We envision the future use of fully biodegradable Si–polymer composite implants that have tailored release characteristics. For example, the development of Si–polymer hybrid materials could lead to the development of environmentally responsive, pulsatile drug release systems that are able to sense the need for a drug and release the required amount of a therapeutic molecule accordingly.

Financial & competing interests disclosure

Support from the Australian Research Council (Australian Capital Territory, Australia), Bellberry Ltd. (Dulwich, South Australia), Flinders University (Adelaide, Australia) and the National Health and Medical Research Council (Canberra, Australia) is gratefully acknowledged. The authors have no other relevant affiliations or financial involvement with any organization or entity with a financial interest in or financial conflict with the subject matter or materials discussed in the manuscript apart from those disclosed.

No writing assistance was utilized in the production of this manuscript.

Ethical conduct of research

The authors state that they have obtained appropriate institutional review board approval or have followed the principles outlined in the Declaration of Helsinki for all human or animal experimental investigations. In addition, for investigations involving human subjects, informed consent has been obtained from the participants involved.

Executive summary

- Mesoporous porous silicon-based materials are attractive candidates for biomedical applications as they are easily modifiable with a wide variety of chemical moieties.
- Encapsulation of porous silicon with polymers can help improve the biocompatibility, tune the biodegradation and drug release kinetics.
- Production of fully biodegradable monolithic composites, such as those described in this article, can potentially facilitate the site-specific release of drugs, without the need for surgical recovery of the device after their payload is exhausted.
- The use of composite materials could help improve drug stability and increase the bioavailability at the site of delivery.
- The composite morphology can be used to control the drug release rate from less than 1 day (surface-grafted poly(L-lactide) [PLLA] composites) to weeks (spin-coated PLLA composites) and even many months (monolithic PLLA materials).
- Release of the small molecular model drug camptothecin from the monolithic PLLA materials was effective at inducing cell death with less than 5% of cells remaining when compared with the negative control after 5 days.

References

Papers of special note have been highlighted as:
- ▪ of interest
- ▪▪ of considerable interest

1 Castro G, Panilaitis B, Kaplan D. Emulsan, a tailorable biopolymer for controlled release. *Bioresour. Technol.* 99(11), 4566–4571 (2008).

2 Hughes G. Nanostructure-mediated drug delivery. *Nanomed. Nanotechnol. Biol. Med.* 1(1), 22–30 (2005).

3 Peng P, Kumar S, Voelcker NH, Szili E, Smart RSC, Griesser HJ. Thin calcium phosphate coatings on titanium by electrochemical deposition in modified simulated body fluid. *J. Biomed. Mater. Res. Part A* 76, 347–355 (2006).

4 Batra I, Coffer J, Canham L. Electronically-responsive delivery from a calcified mesoporous silicon structure. *Biomed. Microdevices* 8, 93–97 (2006).

5 Bikram M, Gobin A, Whitmire R, West J. Temperature-sensitive hydrogels with SiO_2-Au nanoshells for controlled drug delivery. *J. Control. Release* 123, 219–227 (2007).

6 He J, Chen J-Y, Wang P *et al.* Poly(*N*-isopropylacrylamide)-coated thermo-responsive nanoparticles for controlled delivery of sulfonated Zn-phthalocyanine in Chinese hamster ovary cells *in vitro* and zebra fish *in vivo*. *Nanotechnology* 18(41), 415101 (2007).

7 Koh Y, Jang S, Kim J *et al.* DBR pSi/PMMA composite materials for smart patch application. *Colloids Surf. A* 313–314, 328–331 (2008).

▪ **Composites of photonic porous silicon (pSi) and polymers were used to create a self-reporting release system, which could be monitored in real time during *in vivo* applications.**

8 Lin M, Wang H, Meng S *et al.* Structure and release behavior of PMMA/silica composite drug delivery system. *J. Pharm. Sci.* 96(6), 1518–1526 (2007).

9 Song SW, Hidajat K, Kawi S. pH-Controllable drug release using hydrogel encapsulated mesoporous silica. *Chem. Commun.* 42, 4396–4398 (2007).

10 Andreadis S, Geer D. Biomimetic approaches to protein and gene delivery for tissue regeneration. *Trends Biotechnol.* 24(7), 331–337 (2006).

11 Elvira C, Gallardo A, San Roman J, Cifuentes A. Covalent polymer–drug conjugates. *Molecules* 10, 114–125 (2005).

12 Sharma S, Jasper Nijdam A, Sinha P *et al.* Controlled-release microchips. *Expert Opin. Drug Deliv.* 3(3), 379–394 (2006).

13 Soppimath K, Aminabhavi T, Kulkarni A, Rudzinski W. Biodegradable polymeric nanoparticles as drug delivery devices. *J. Control. Release* 70(1–2), 1–20 (2001).

14 Wood K, Boedicker J, Lynn D, Hammond P. Tunable drug release from hydrolytically degradable layer-by-layer thin films. *Langmuir* 21(4), 1603–1609 (2005).

15 Tsukagoshi T, Kondo Y, Yoshino N. Preparation of thin polymer films with controlled drug release. *Colloids Surf. B* 57(2), 219–225 (2007).

16 Smith JR, Smith RD, Holland GN *et al.* Differential efficacy of tumor necrosis factor inhibition in the management of inflammatory eye disease and associated rheumatic disease. *Arthritis Care Res.* 45, 252–257 (2001).

17 Jabs DA, Rosenbaum JT, Foster CS *et al.* Guidelines for the use of immunosuppressive drugs in patients with ocular inflammatory disorders: recommendations of an expert panel. *Am. J. Ophthalmol.* 130(4), 492–513 (2000).

18 Jap A, Chee S-P. Immunosuppressive therapy for ocular diseases. *Curr. Opin. Ophthalmol.* 19, 535–540 (2008).

19 Leske MC. Open-angle glaucoma: an epidemiologic overview. *Ophthal. Epidemiol.* 14, 166–172 (2007).

20 Rolim De Moura CR, Paranhos A Jr, Wormald R. Laser trabeculoplasty for open angle glaucoma. *Cochrane Rev.* 4, CD003919 (2009).

21 Vass C, Hirn C, Sycha T *et al.* Medical interventions for primary open angle glaucoma and ocular hypertension. *Cochrane Rev.* 4, CD003167 (2009).

22 Chang J-H, Gabison EE, Kato T, Azar DT. Corneal neovascularization. *Curr. Opin. Ophthalmol.* 12, 242–249 (2001).

23 Canham LT. Bioactive silicon structure fabrication through nanoetching techniques. *Adv. Mater.* 7(12), 1033–1037 (1995).

24 Canham L, Aston R. Will a chip everyday keep the doctor away? *Phys. World* 14, 27–31 (2001).

25 *Properties of Porous Silicon*. Canhan L (Ed.). Short Run Press, London, UK (1997).

26 Park J-H, Gu L, Maltzahn GV, Ruoslahti E, Bhatia SN, Sailor MJ. Biodegradable luminescent porous silicon nanoparticles for *in vivo* applications. *Nat. Mater.* 8, 331–336 (2009).

27 Schwartz M, Cunin F, Cheung R, Sailor M. Chemical modification of silicon surfaces for biological applications. *Phys. Status Solid. A* 202(8), 1380–1384 (2005).

28 Letant S, Kane S, Hart B *et al.* Hydrolysis of acetylcholinesterase inhibitors – organophosphorous acid anhydrase enzyme immobilization on photoluminescent porous silicon platforms. *Chem. Commun.* 7, 851–853 (2005).

29 Thomas J, Pacholski C, Sailor M. Delivery of nanogram payloads using magnetic porous silicon microcarriers. *Lab Chip* 6, 782–787 (2006).

30 Anglin E, Schwartz M, Ng V, Perelman L, Sailor M. Engineering the chemistry and nanostructure of porous silicon Fabry–Perot films for loading and release of a steroid. *Langmuir* 20(25), 11264–11269 (2004).

31 Anglin E, Cheng L, Freeman W, Sailor M. Porous silicon in drug delivery devices and materials. *Adv. Drug Deliv. Rev.* 60, 1266–1277 (2008).

▪▪ **Provides an excellent overview of the use of pSi devices for drug delivery applications.**

32 McInnes SJP, Voelcker NH. Silicon–polymer hybrid materials for drug delivery. *Future Med. Chem.* 1(6), 1051–1074 (2009).

▪▪ **Provides an excellent overview of the use of silicon-based composite materials for drug delivery applications.**

33 Prestidge C, Barnes T, Lau C-H, Barnett C, Loni A, Canham L. Mesoporous silicon: a platform for the delivery of therapeutics. *Expert Opin. Drug Deliv.* 4(2), 101–110 (2007).

34 Cheng L, Anglin E, Cunin F *et al.* Intravitreal properties of porous silicon photonic crystals: a potential self-reporting intraocular drug delivery vehicle. *Br. J. Opthalmol.* 92, 705–711 (2008).

35 Dorvee J, Derfus A, Bhatia S, Sailor M. Manipulation of liquid droplets using amphiphilic, magnetic one-dimensional photonic crystal chaperones. *Nat. Mater.* 3, 896–899 (2004).

36 Low S, Williams K, Canham L, Voelcker N. Evaluation of mammalian cell adhesion on surface-modified porous silicon. *Biomaterials* 27(26), 4538–4546 (2006).

37 Low SP, Voelcker NH, Canham LT, Williams KA. The biocompatibility of porous silicon in tissues of the eye. *Biomaterials* 30, 2873–2880 (2009).

▪▪ **Provides evidence for the compatibility of pSi-based devices in ophthalmological applications.**

38 McInnes SJP, Thissen H, Choudhury N, Voelcker N. New biodegradable materials produced by ring opening polymerisation of poly(L-lactide) on porous silicon substrates. *J. Colloid Interface Sci.* 332(2), 336–344 (2009).

▪▪ **Provides further experimental details of the surface-initiated ring opening polymerization of poly(L-lactide) to porous silicon surfaces.**

39 Maretschek S, Greiner A, Kissel T. Electrospun biodegradable nanofiber nonwovens for controlled release of proteins. *J. Control. Release* 127, 180–187 (2008).

40 Mundargi RC, Srirangarajan S, Agnihotri SA *et al.* Development and evaluation of novel biodegradable microspheres based on poly(D,L-lactide-co-glycolide) and poly(ε-caprolactone) for controlled delivery of doxycycline in the treatment of human periodontal pocket: *in vitro* and *in vivo* studies. *J. Control. Release* 119, 59–68 (2007).

41 Youxin L, Volland C, Kissel T. *In vitro* degradation and bovine serum albumin release of the ABA triblock copolymers consisting of poly (L(+) lactic acid), or poly (L(+) lactic acid-co-glycolic acid) A-blocks attached to central polyoxyethylene B-blocks. *J. Control. Release* 32, 121–128 (1994).

42 Robert L. New methods of drug delivery. *Science* 249, 1527–1533 (1990).

43 Choi I, Langer R. Surface-initiated polymerization of L-lactide: coating of solid substrates with a biodegradable polymer. *Macromolecules* 34, 5361–5363 (2001).

44 Kowalski A, Duda A, Penczek S. Kinetics and mechanism of cyclic esters polymerization initiated with tin(II) octoate. 3: polymerization of L,L-dilactide. *Macromolecules* 33, 7359–7370 (2000).

▪ **Provides insight into the mechanism of polymerization of polylactides.**

45 Langer R. Biomaterials in drug delivery and tissue engineering: one laboratory's experience. *Acc. Chem. Res* 33, 94–101 (2000).

46 Lee W, Lee J, Ha C. Growth of monolayered poly(L-lactide) lamellar crystals on a substrate. *Macromol. Res.* 11(6), 511–513 (2003).

47 Panyam J, Labhasetwar V. Sustained cytoplasmic delivery of drugs with intracellular receptors using biodegradable nanoparticles. *Mol. Pharmaceutics* 1(1), 77–84 (2004).

48 Tasaka F, Ohya Y, Ouchi T. Synthesis of novel comb-type polylactide and its biodegradability. *Macromolecules* 34, 5494–5500 (2001).

49 Yoon K, Koh Y, Choi I *et al.* Surface-initiated, ring-opening polymerisation of p-dioxanone from gold and silicon oxide surfaces. *J. Mater. Chem* 13, 2910–2914 (2003).

50 Albertsson A, Varma I. Recent developments in ring opening polymerisation of lactones for biomedical applications. *Biomacromolecules* 4, 1466–1486 (2003).

51 Andreopoulos A, Hatzi E, Doxastakis M. Controlled release of salicylic acid from poly(D,L-lactide). *J. Mater. Sci. Mater. Med.* 12, 233–239 (2001).

52 Lehninger A, Nelson D, Cox M. *Principles of Biochemistry.* Worth Publishers, NY, USA (1993).

53 Zhang Y, Chu C. Biodegradable dextran-polylactide hydrogel networks: their swelling, morphology and the controlled release of indomethacin. *Biomed. Mater. Res.* 59, 318–328 (2002).

54 Jain RA. The manufacturing techniques of various drug loaded biodegradable poly(lactide-co-glycolide) (PLGA) devices. *Biomaterials* 21, 2475–2490 (2000).

55 Uhrich KE, Cannizzaro SM, Langer RS, Shakesheff KM. Polymeric systems for controlled drug release. *Chem. Rev.* 99, 3181–3198 (1999).

56 Dong WY, Körber M, Esguerra VL, Bodmeier R. Stability of poly(D,L-lactide-co-glycolide) and leuprolide acetate in in-situ forming drug delivery systems. *J. Control. Release* 115, 158–167 (2006).

57 Cheng L, Anglin E, Cunin F *et al.* Intravitreal properties of porous silicon photonic crystals: a potential self-reporting intraocular drug-delivery vehicle. *Br. J. Opthalmol.* 92(5), 705–711 (2008).

58 Armarego W, Perrin D. *Purification of Laboratory Chemicals, 4th Edition*. Butterworth-Heinemann, Oxford, UK (1996).

59 Zhao X, Zu Y, Li Q *et al.* Preparation and characterization of camptothecin powder micronized by a supercritical antisolvent (SAS) process. *J. Supercritical Fluids* 51, 412–419 (2010).

60 Sigma-Aldrich. *(S)-(+)-Camptothecin material Safety Data Sheet.* Sigma-Aldrich Pty. Ltd. Castle Hill, NSW, Australia (2010).

61 Sætern AM, Nguyen NB, Bauer-Brandl A, Brandl M. Effect of hydroxypropyl–cyclodextrin-complexation and pH on solubility of camptothecin. *Int. J. Pharm.* 284, 61–68 (2004).

62 Basak SC, Kumar KS, Ramalingam M. Design and release characteristics of sustained release tablet containing metformin HCl. *Braz. J. Pharm. Sci.* 44(3), (2008).

63 Bhattacharyya S, Ray S, Gupta BK, Ghosh LK. Design, evaluation and statistical optimisation of a controlled release multiparticulate acyclovir delivery system. *Lat. Am. J. Pharm.* 26(6), 852–858 (2007).

64 Dave BS, Amin AF, Patel MM. Gastroretentive drug delivery system of ranitidine hydrochloride: formulation and *in vitro* evaluation. *AAPS PharmSci. Tech.* 5(2), e34 (2004).

65 Naeem M, Mahmood A, Khan S, Shahiq Z. Development and evaluation of controlled-release bilayer tablets containing microencapsulated tramadol and acetaminophen. *Trop. J. Pharm. Res.* 9(4), 347–354 (2010).

66 Nie S, Hsiao WW, Pan W, Yang Z. Thermoreversible Pluronic® F127-based hydrogel containing liposomes for the controlled delivery of paclitaxel: *in vitro* drug release, cell cytotoxicity, and uptake studies. *Int. J. Nanomed.* 6, 151–166 (2011).

67 Poovi G, Lekshmi UD, Narayanan N, Reedy P. Preparation and characterisation of repaglinide loaded chitosan polymeric nanoparticles. *Res. J. Nanosci. Nanotechnol.* 1(1), 12–24 (2011).

68 Ravi PR, Ganga S, Saha RN. Design and study of lamivudine oral controlled release tablets. *AAPS PharmSci. Tech.* 8(4), E101 (2007).

69 Mirji SA, Halligudi SB, Mathew N, Ravia V, Jacob NE, Patil KR. Adsorption of methanol on Si(100)/SiO_2 and mesoporous SBA-15. *Colloids Surf. A* 287, 51–58 (2006).

70 Meaurio E, Lopez-Rodriguez N, Sarasua JR. Infrared spectrum of poly(L-lactide): application to crystallinity studies. *Macromolecules* 39, 9291–9301 (2006).

71 Dubois P, Jacobs C, Jerome R, Teyssie P. Macromolecular engineering of polylactones and polylactides. 4: Mechanism and kinetics of lactide homopolymerization by aluminum isopropoxide. *Macromolecules* 24, 2266–2270 (1991).

72 Goffin A-L, Duquesne E, Moins S, Alexandre M, Dubois P. New organic–inorganic nanohybrids via ring opening polymerization of (di)lactones initiated by functionalized polyhedral oligomeric silsesquioxane. *Eur. Polym. J.* 43, 4103–4113 (2007).

73 Cam D, Marucci M. Influence of residual monomers and metals on poly(L-lactide) thermal stability. *Polymer* 38(8), 1879–1884 (1997).

74 Fleurya F, Kudelinab I, Nabieva I. Interactions of lactone, carboxylate and self-aggregated forms of camptothecin with human and bovine serum albumins. *FEBS Letters* 406, 151–156 (1997).

75 Wall ME, Wani MC, Cook CE, Palmer KH, Mcphail AT, Sim GA. Plant anti-tumor agents. I. The isolation and structure of campthothecin, a novel alkaloidal leukemia and tumor inhibitor from *Camptohtheca acuminata*. *J. Am. Chem. Soc.* 88(16), 3888–3890 (1966).

76 Kanga J, Kumara V, Yanga D, Chowdhurya PR, Hohlb RJ. Cyclodextrin complexation: influence on the solubility, stability, and cytotoxicity of camptothecin, an antineoplastic agent. *Eur. J. Pharm. Sci.* 15, 163–170 (2002).

77 Abraham LM, Selva D, Casson R, Leibovitch I. Mitomycin: clinical applications in ophthalmic practice. *Drugs* 66(3), 321–340 (2006).

78 Li Y, Cunin F, Link J *et al.* Polymer replicas of photonic porous silicon for sensing and drug delivery applications. *Science* 299, 2045–2047 (2003).

79 Dash S, Murthy PN, Nath L, Chowdhury P. Kinetic modeling on drug release from controlled drug delivery systems. *Acta Poloniae Pharmaceutica Drug Res.* 67(3), 217–233 (2010).

80 Higuchi T. Rate of release of medicaments from ointment based containing drugs in suspension. *J. Pharm. Sci.* 50, 847 (1961).

81 Higuchi T. Mechanism of sustained-action medication. Theoretical analysis of rate of release of solid drugs dispersed in solid matrices. *J. Pharm. Sci.* 52(12), 1145 (1963).

82 Hixson A, Crowell J. Dependence of reaction velocity upon surface and agitation. *Ind. Eng. Chem.* 23(8), 923–931 (1931).

83 Ritger PL, Peppas NA. A simple equation for description of solute release II. Fickian and anomalous release from swellable devices. *J. Control. Release* 5, 37–42 (1987).

84 Ritger PL, Peppas NA. A simple equation for description of solute release I. Fickian and non-Fickian release from non-swellable devices in the form of slabs, spheres, cylinders or discs. *J. Control. Release* 5, 23–36 (1987).

85 Desai SJ, Simonelli AP, Higuchi WI. Investigation of factors influencing release of solid drug dispersed in inert matrices. *J. Pharm. Sci.* 54, 1459–1464 (1965).

86 Desai SJ, Singh P, Simonelli AP, Higuchi WI. Investigation of factors influencing release of solid drug dispersed in inert matrices II. *J. Pharm. Sci.* 55, 1224–1229 (1966).

87 Andersson J, Rosenholm J, Areva S, Linden M. Influences of material characteristics on ibuprofen drug loading and release profiles from ordered micro- and mesoporous silica matrices. *Chem. Mater.* 16, 4160–4167 (2004).

88 Shoaib MH, Tazeen J, Merchant HA, Yousuf RI. Evaluation of drug release kinetics from ibuprofen matrix release tablets using HPMC. *Pak. J. Pharm. Sci.* 19(2), 119–124 (2006).

89 Peppas NA. Analysis of Fickian and non-Fickian drug release from polymers. *Pharm. Acta Helv.* 60(4), 110–111 (1985).

90 Peel MR, Milstead MW, Sternbach DD *et al.* Novel A-ring modified camptothecins as topoisomerase I inhibitors. *Bioorganic Med. Chem. Lett.* 5(18), 2129–2132 (1995).

91 Yang F, Xu C, Kotaki M, S. W, Ramakrishna S. Characterisation of neutral stem cells on electrospun poly(L-lactic acid) nanofibrous scaffold. *J. Biomater. Sci. Polymer Ed.* 15(12), 1483–1497 (2004).